Geologia Sudetica, 2006, 38: 39–61.

Fractional crystallization, mafic replenishment and assimilation in crustal magma chambers: geochemical constraints from the Permian post-collisional intermediate-composition volcanic suite of the North-Sudetic Basin (SW Poland)

Marek Awdankiewicz

University of Wrocław, Institute of Geological Sciences, Department of Mineralogy and Petrology, ul. Cybulskiego 30, 50-205 Wrocław, Poland; email: mawdan@ing.uni.wroc.pl

Key words: petrology, basaltic andesites, post-collisional volcanism, Sudetes

Abstract The Permian intermediate-composition lavas of the North-Sudetic Basin represent a high-K calc-alkaline suite emplaced in an extensional, intracontinental, post-collisional setting in the eastern part of the European Variscan belt. The lavas, in a total volume of over 100 km^3, erupted from fissure vents or small shield-type volcanoes in several episodes separated by repose and sedimentation periods. An idealised eruptive episode comprised basaltic trachyandesites (plagioclase-phyric, clinopyroxene lavas) followed by predominant, main-series basaltic andesites (weakly porphyrytic, two-pyroxene microcrystalline lavas) and evolved basaltic andesites (weakly porphyrytic, two-pyroxene fine-grained lavas). This volcanic suite originated in magmatic systems where differentiation processes evolved with time from (I) fractional crystallization, producing the basaltic trachyandesites, through (II) fractional crystallization coupled with mafic replenishment, resulting in the main series basaltic andesite lavas, to (III) fractional crystallization, mafic replenishment and minor crustal contamination, producing the evolved basaltic andesites. The fractionating mineral assemblages changed during the successive stages and, apart from plagioclase, olivine, clinopyroxene and Fe-Ti oxides, included orthopyroxene (stage II and III) and apatite with zircon (stage III). The general trace element characteristics of the volcanic rocks (enrichment in Th, LILE, Nb and Zr, but with high Th/Nb and La/Nb ratios) are transitional between those of extension-related within-plate lavas and active continental margin lavas. These characteristics are inherited from enriched lithospheric mantle sources carrying a crustal signature related to subduction processes during the earlier stages of the Variscan orogeny.

Manuscipt received 21 May 2006, accepted 16 October 2006

INTRODUCTION

Post-collisional volcanism is characterized by a wide geochemical variation of erupted magmas which derive from various mantle and crustal sources and evolve through a range of shallow-level differentiation processes. Calc-alkaline to high-K calc-alkaline volcanic rocks are widespread in post-collisional settings, and particularly typical of the early post-collisional period, as has been well established in several Cenozoic to Recent settings (e.g. Anatolia, Carpathians and Oranie, Algeria; Aldanmaz *et al.*, 2000; Seghedi *et al.*, 2001; Coulon *et al.*, 2002), and also recognized in the Permo-Carboniferous volcanic province of Europe (e.g. Lorenz & Nicholls, 1976, 1984; Menard & Molnar, 1988; Cabanis *et al.*, 1990; Benek *et al.*, 1996; Awdankiewicz, 1999a, b; Romer *et al.*, 2001). It is generally considered that basic magmas in such suites originate from subduction-modified lithospheric mantle sources, and further evolve through assimilation and fractionation processes in crustal magma chambers. However, in many cases, the petrogenetic processes that operate at the scale of individual volcanic fields or centres are not constrained in detail, even though 1) they significantly contribute to the overall geochemical variation, and 2) understanding them may be critical for the distinction between deep- and shallow-level phenomena resulting in similar geochemical signatures of magmas, e.g. source contamination vs. wall rock assimilation by ascending and fractionating magmas. The latter issue is of particular importance in the case of many late Palaeozoic volcanic successions of western-central Eu-

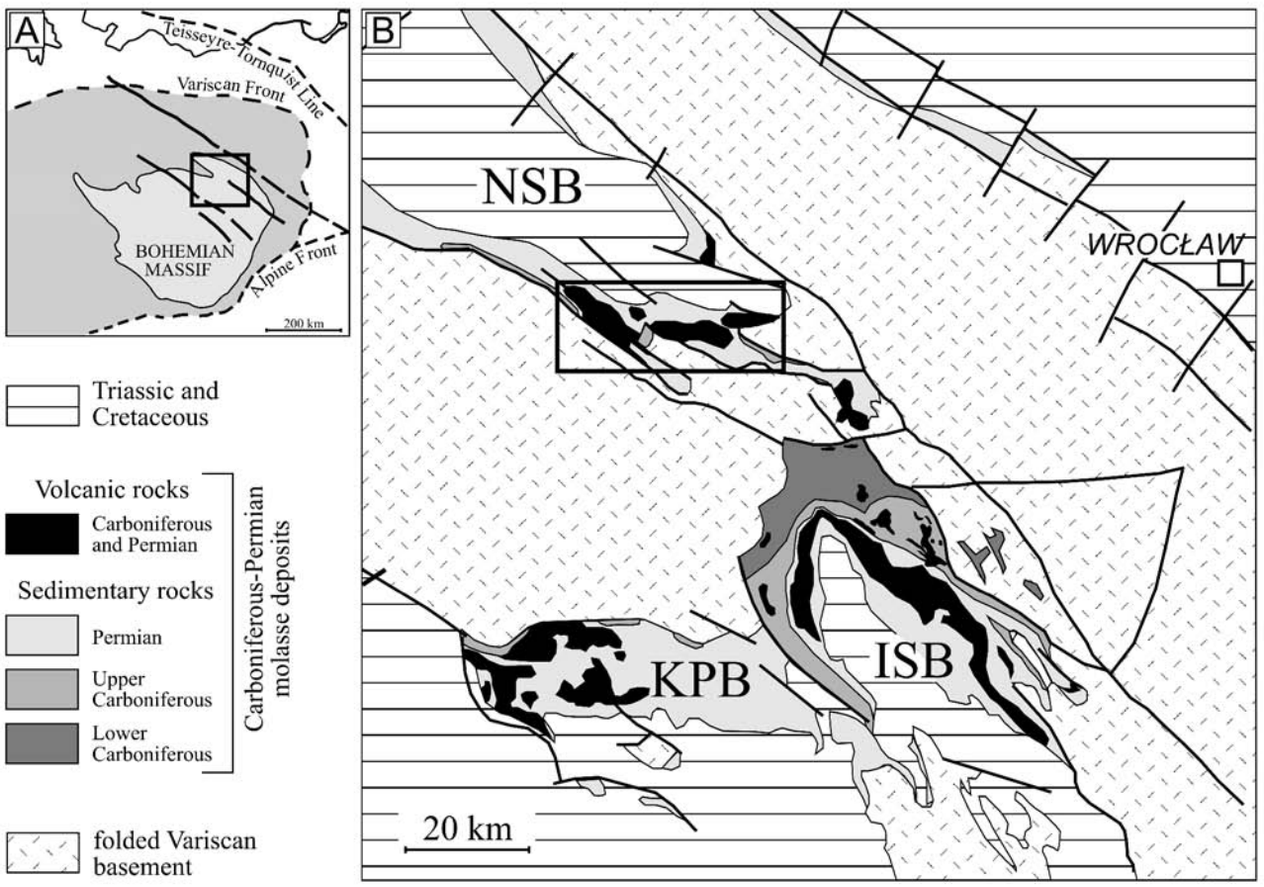

Fig. 1. A. The location of the Sudetes (frame) within the Variscan Belt of Europe. **B.** A geological sketch of the Sudetes area (without Cenozoic deposits) showing the distribution of the late Palaeozoic intramontane troughs (NSB – North-Sudetic Basin, ISB – Intra-Sudetic Basin, KPB – Krkonoše Piedmont Basin) and the location of the study area (frame).

rope, where primitive mantle-derived basic rocks are rare or absent (e.g. Wilson *et al.*, 2004; Ulrych *et al.*, 2006) and the origin of the specific geochemical signatures of the volcanic rocks is still debatable.

A well-exposed suite of post-collisional, Permian lavas of intermediate composition ("melaphyres") crops out in the North-Sudetic Basin, a late Palaeozoic intramontane trough in the eastern part of the Variscan Belt of Europe (Fig. 1). In this paper, the geological and palaeovolcanological context of these volcanic rocks is briefly outlined and followed by a more detailed petrographic, mineralogical and geochemical characterization. The aim of this paper is to present the numerical modelling of the trace element variation and a discussion thereof. This trace element variation puts constraints on both the shallow-level differentiation processes (fractional crystallization, mafic replenishment and crustal assimilation) and on the mantle sources involved in the petrogenesis of this suite.

THE GEOLOGICAL BACKGROUND TO THE PERMIAN VOLCANISM IN THE SUDETES AND THE NORTH-SUDETIC BASIN

The Sudetes are a mountain range located in SW Poland, at the NE margin of the Bohemian Massif (Fig. 1A). The Neoproterozoic to Lower Carboniferous, largely crystalline rock complexes that crop out extensively in the Sudetes region represent the easternmost parts of the European Variscan Belt (e.g. Franke & Żelaźniewicz, 2000; Aleksandrowski *et al.*, 2000; Mazur *et al.*, 2006 and references therein). During Middle Devonian to Early Carboniferous times, the Variscan orogenic processes culminated with a continental collision associated with, and followed by, a period of extensional tectonics, featuring the formation of intramontane troughs, the accumulation of thick molasse successions, and intense volcanic activity. In the Sudetes, this volcanism reached its climax in early Permian times (e.g. Awdankiewicz, 1999a, b and references therein) and represented a distinctive, post-collisional, extension-related magmatic episode.

In particular, the North-Sudetic Basin is one of three major late Palaeozoic intramontane troughs of the Sudetes area (Fig. 1B). This basin is a fault-bounded, NW–SE trending synclinorial structure with several grabens and horsts in its eastern and southern parts. The basement of the basin is represented by the Kaczawa Complex, a Variscan accretionary prism composed of Cambrian (?) to

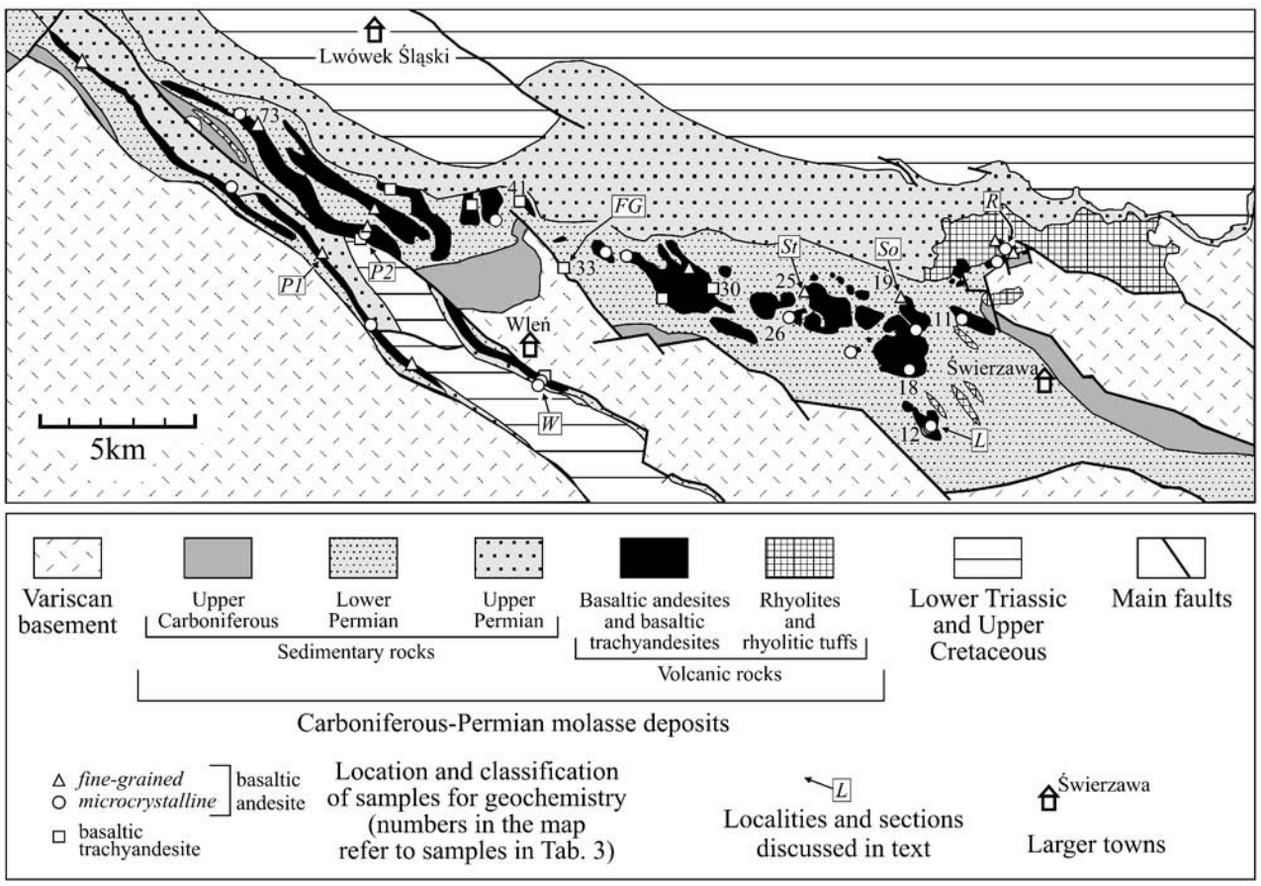

Fig. 2. A geological sketch of the study area (without Cenozoic, modified from Kozłowski and Parachoniak, 1967). Localities and sections discussed in the text: FG – Folwarczna Góra, an old quarry 300 m NW of the top of the hill; L – Lubiechowa, an old quarry on Łomy hill; P1 – Pławna 1, a railway cut ca. 900 m WSW of Pławna Średnia station; P2 – Pławna 2, a railway cut and an old quarry at 320.8 hill in the northern part of Pławna village; R – Różana, rock crags on the eastern bank of the Kaczawa river, ca. 1 km north of Różana; So – Sokołowiec, rock crags on the eastern bank of the Czernica stream, ca. 250 m SSW of a major road junction (Sokołowiec-Sędziszowa); St – Stefanów village, small rocks on a hill slope 1100 m NW of Łysa Góra hill; W – Wleń, extensive (ca. 300 m) rock crags SE and SW of the railway tunnel.

Visean, low grade (up to blueschist and greenschist facies) metasedimentary and metavolcanic rocks (Baranowski *et al.*, 1990; Collins *et al.*, 2000, and references therein). The North-Sudetic Basin fill comprises the uppermost Carboniferous (Stephanian) to Lower Permian continental volcano-sedimentary succession, overlain by uppermost Permian (Zechstein), Lower Triassic and Upper Cretaceous marine deposits. The Lower Permian deposits are ca. 1 km thick and consist largely of siliciclastic sedimentary rocks that accumulated in alluvial and lacustrine environments (Wojewoda and Mastalerz, 1989). Thick intercalations of volcanic rocks in the middle part of the succession are grouped into an informal unit known as the Lower Permian Volcanic Complex (Milewicz, 1965; Kozłowski and Parachoniak, 1967).

The Lower Permian volcanic rocks crop out along the southern and eastern margins of the North-Sudetic Basin (Fig. 1B). In the study area (Fig. 2), the volcanic complex predominantly comprises intermediate-composition rocks (traditionally known as "melaphyres", and later usually classified as trachybasalts), with less widespread acidic volcanics in the east. Kozłowski and Parachoniak (1967) suggested that the complex formed in two cycles of volcanic activity with intermediate lavas followed by acidic lavas and/or tuffs in each cycle. However, the older of these two "cycles" has a very limited lateral extent. It is only recognized west of Świerzawa, and is represented by a single, small "trachybasalt" outcrop and three thin "rhyolitic tuff" intercalations a few metres thick each (not exposed, known from trenches only). The rest of the intermediate rocks belong to the "second cycle". However, north of Świerzawa, these intermediate rocks straddle and cross-cut the boundaries of the acidic volcanogenic rocks and the host sedimentary rocks, and in part may represent subvolcanic intrusions younger than the rhyolitic rocks, and not lavas emplaced prior to the rhyolites, as considered by Kozłowski and Parachoniak (1967). Thus, the concept of "volcanic cycles" of Kozłowski and Parachoniak seems to be not well supported. It is rather considered here that the intermediate-composition rocks reflect a major, polyphase effusive stage of the Permian mafic volcanism in the North-Sudetic Basin. The relationships of the mafic and felsic rocks remain poorly constrained.

THE SCOPE OF THIS STUDY AND THE METHODS USED

This study deals with the intermediate-composition volcanic rocks of the North-Sudetic Basin, and it is focused on the following objectives: 1) the emplacement processes of the volcanic rocks and the style of activity of the Permian volcanoes in the area; 2) the petrographic and geochemical characterization of the volcanic rocks and their variation in space and time; and 3) the origin of magmas, in particular their differentiation processes. Field studies included systematic sampling and logging of the best-exposed sections of the volcanic rocks. Approximately 100 samples were collected and examined in thin sections, and the freshest specimens were selected for chemical analyses. The major and trace element compositions of 43 samples were determined at Keele University, UK, via the XRF method using an ARL 8420 spectrometer. Details on the analytical methods and their precision and accuracy are given in Floyd and Castillo (1992). 10 representative samples were analysed for Cs, Hf, Sc, Ta, Th, U and the rare earth elements using the INAA method at Activation Laboratories Ltd, Canada (2MW Pool Type reactor, Ge ORTEC and CANBERRA gamma detectors). The accuracy of these results is better than ± 10% (all the elements show concentrations at levels of 10 to 100x the detection limit of the method used). The mineral chemistry was determined in 4 samples using the Cambridge Microscan 5 electron microprobe (WDS technique) at the Institute of Geological Sciences, University of Wrocław. The typical analytical conditions were: counting time 20 s, beam current 50 nA and accelerating voltage 15 kV.

THE PALAEOVOLCANOLOGY AND EMPLACEMENT PROCESSES OF THE VOLCANIC ROCKS

The Permian intermediate-composition volcanic rocks of the North-Sudetic Basin crop out within an area measuring ca. 30 km from west to east and 10 km from north to south. The thickness of the volcanic rocks ranges from tens to hundreds of metres and attains a maximum total value of ca. 0.5 km in the western-central part of the area near Pławna (Kozłowski and Parachoniak, 1967). The erupted volume of the intermediate magmas can thus be roughly estimated at up to ca. 150 km^3 within the study area and, possibly, up to several hundreds of cubic kilomtres within the whole North-Sudetic Basin. These intermediate-composition rocks are lava flows and shallow-level subvolcanic intrusions (laccoliths), and no equivalent pyroclastic deposits have been found. This suggests that the eruptive centres were small shield-type volcanoes or fissure vents. However, their location remains unconstrained, as no evidence of dykes, vents or near-vent deposits has been discerned thusfar.

The intermediate volcanic rocks laterally and up-sequence interdigitate with sedimentary clastic rocks. In particular, 5 successive volcanic horizons are found within the Lower Permian strata in the western part of the study area between Lwówek Śląski and Wleń, around Pławna (Fig. 2). Furthermore, many of the well-exposed sections of the volcanic rocks consist of several stacked lava sheets, e.g. 7 lava sheets occur at Lubiechowa, 5 at Wleń, 3 at Folwarczna Góra, and at least 2 at several other localities. These relationships show that: 1) the volcanic activity comprised several eruptive episodes separated by repose and sedimentation periods; and 2) multiple effusions of lavas occurred during most of the eruptive episodes.

Representative logs of well-exposed sections are shown in Fig. 3A. The individual lava sheets are usually 10–20 m thick, with massive lower portions and vesicular to amygdaloidal upper parts (Fig. 4A). Blocky, platy and irregular joints are most typical. Occasionally, lava breccias or poorly preserved ropy structures are found on top of the sheets. A tree trunk imprint recognized as Calamites sp. (P. Raczyński, pers. com.) was found in a lava at Lubiechowa. The described lava sheets may largely represent pahoe-hoe flows (e.g. Sokołowiec section in Fig. 3A), and more rarely aa or block lavas. In addition, pillow-like structures (Fig. 4B), small patches of peperites, sedimentary intercalations, xenoliths and clastic dykes are found at some localities (e.g. at Lubiechowa, Płóczki Górne, Gradówek, and in the Różana area). These features indicate that lava-wet sediment interactions locally accompanied the emplacement of the intermediate rocks. These interactions might have occurred when lavas flowed over wet, muddy ground or sank into unconsolidated deposits as invasive flows (e.g. the Lubiechowa section). Some other igneous bodies were possibly emplaced as shallow-level intrusions (cryptodomes and/or small laccoliths) within wet, poorly consolidated sediments. Such intrusions may be more common in the north-eastern part of the study area, near Różana, where there are several outcrops that are oval in shape and some which may be locally discordant relative to the lithological boundaries within their country rocks.

THE DISTRIBUTION AND ERUPTIVE SEQUENCE OF THE VOLCANIC ROCKS

Petrographically and geochemically, the studied volcanic rocks are subdivided into three main types: 1) microcrystalline basaltic andesites; 2) fine-grained basaltic andesites; and 3) basaltic trachyandesites (Tab. 1, details in the following chapters). The distribution of these rock types is tentatively illustrated in Fig. 2. It is not mapped in detail because: 1) there is both lateral and vertical variation in several outcrops; and 2) these volcanic rocks can barely

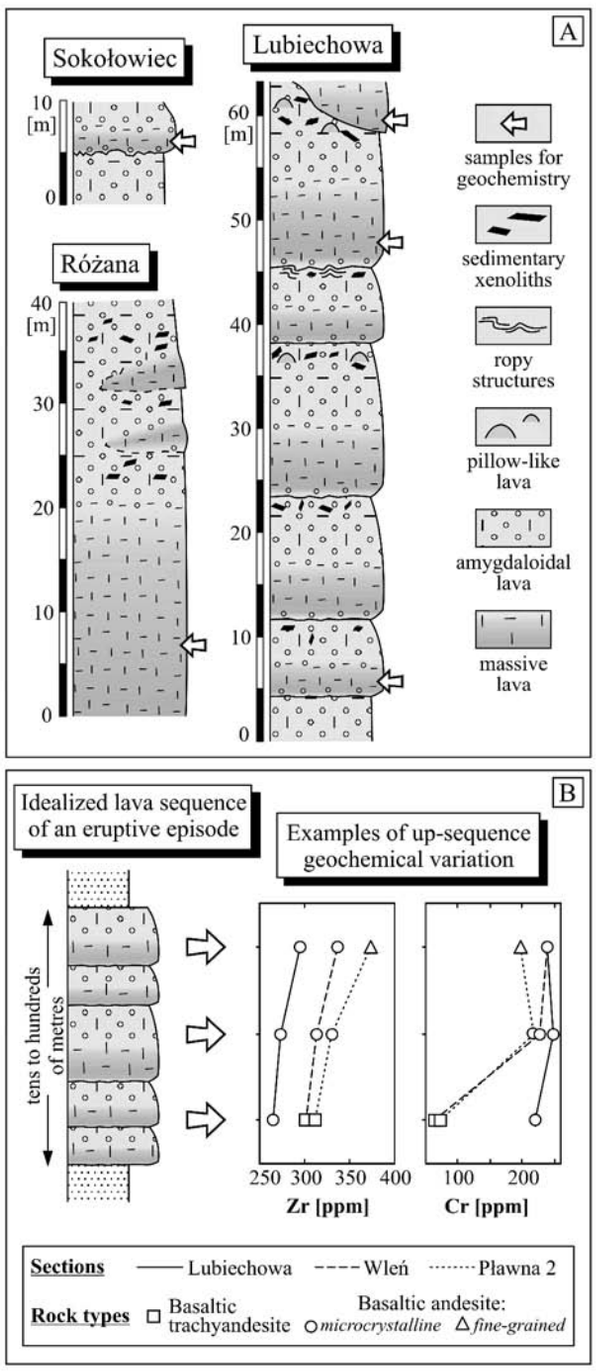

Fig. 3. A. Representative field logs of the volcanic rocks. **B.** An idealized sequence of lavas emplaced during an eruptive episode with examples of up-sequence geochemical variation. The location of the sections shown in (A) and (B) is indicated in Fig. 2.

Fig. 4. Structures of basaltic andesite lava flows at Lubiechowa. A. The contact of two successive lava flows in the lower part of the succession. The upper part of the lower flow (La in the photo) consists of an amygdaloidal lava. The contact (broken line) is sharp and wavy. The basal part of the upper flow consists of a massive lava (Lm). The hammer (for scale) is 30 cm long. B. Pillow-like structures in the upper part of the succession. The pillows are built up of amygdaloidal lavas (La) separated by pockets and veins of fine-grained sandstones (S). The pencil (for scale) is 15 cm long.

be classified in hand-specimens, and much more dense petrographic and geochemical sampling would be required to correlate the various sections.

In general, microcrystalline basaltic andesites predominate across the study area. They are exposed in ca. 50% of the 46 sampled localities. Fine-grained basaltic andesites and basaltic trachyandesites are less common, and are exposed at 35% and 15% of localities, respectively. The eastern part of the study area around Sokołowiec is relatively monotonous. There, the strongly dominant microcrystalline basaltic andesites are only locally accompanied by the fine-grained basaltic andesites, and the basaltic trachyandesites were not observed. By contrast, the central and west-

Table 1

Classification and major petrographic and geochemical characteristics of the intermediate-composition volcanic rocks of the North-Sudetic Basin

ROCK TYPE	PETROGRAPHIC CHARACTERISTICS	GEOCHEMICAL CHARACTERISTICS	
		major elements (TAS*)	trace elements
1. basaltic andesite	weakly porphyrytic, two-pyroxene lavas	basaltic andesites	high-Cr lavas
1a. microcrystalline	microcrystalline	main series basaltic andesites	low Zr/Nb group
1b. fine-grained	fine-grained	evolved basaltic andesites	high Zr/Nb group
2. basaltic trachyandesite	plagioclase-phyric, clinopyroxene lavas	basaltic trachyandesites	low-Cr lavas

** based on fresh samples: LOI < 2%, no alteration of plagioclase and pyroxenes*

ern parts of the study area are characterized by a greater abundance of the fine-grained basaltic andesites and the basaltic trachyandesites.

In some better-exposed sections, petrographical analysis revealed a distinctive succession of rock types. At Stefanów and Pławna1 (locations shown in Fig. 2), the microcrystalline basaltic andesite lava flows are overlain by the fine-grained basaltic andesite lava flows. At Pławna2, the basaltic trachyandesites are exposed near the base of a ca. 100-m thick lava succession, with the microcrystalline basaltic andesites in the middle part, and the fine-grained basaltic andesites towards the top of the sequence. A similar succession of basaltic trachyandesites followed by microcrystalline basaltic andesites (with poorly exposed fine-grained basaltic andesite intercalations ?) was observed in the Wleń section. In addition, an up-sequence geochemical variation was observed at Pławna2, Wleń and Lubiechowa (Fig. 3B and the following chapters).

The discussed relationships show that the composition of the lavas emplaced during an effusive eruptive episode in the North-Sudetic Basin changed with time. It is considered that an idealized, complete eruptive episode consisted of three effusive phases (Fig. 3B):

– the initial, basaltic trachyandesite phase,

– the main, microcrystalline basaltic andesite phase, and

– the final, fine-grained basaltic andesite phase.

This pattern, sometimes incomplete (e.g. without the initial and/or final members) was repeated several times, as volcanic activity resumed after repose periods. Ultimately, this pattern of activity may be interpreted to reflect several magmatic cycles that included 1) episodic generation of mafic magmas at depths, followed by 2) magma supply into, and differentiation within, the plumbing systems of the volcanoes, and 3) eruption of the variably evolved melts (from compositionally zoned plumbing systems ?). The lateral variation of eruptive products (e.g. the lack of basaltic trachyandesites in the east) may reflect some differences in the magmatic evolution and/or eruptive processes at individual volcanic centres.

THE PETROGRAPHY AND MINERAL CHEMISTRY OF THE VOLCANIC ROCKS

The intermediate-composition lavas of the North-Sudetic Basin show rather weak petrographic variation in hand-specimens. The massive rocks typical of lava flow interiors are moderately porphyrytic to aphanitic, dark grey to greenish in colour, and relatively fresh. However, the more common vesicular and amygdaloidal rocks found at the margins of the lava flows are purple to reddish-brown in colour and always show a strong hydrothermal alteration. This alteration resulted in a variable filling of vesicles and the replacement of the primary igneous phases with albite, quartz, carbonates, chlorites, celadonite, smectites and hematite (Kozłowski and Parachoniak, 1967; Kowalska and Michalik, 1996; Awdankiewicz and August, 1998). K-Ar dating of celadonite from amygdales suggests that the alteration processes spanned the late Permian to middle Jurassic period (252.5–177.5 Ma; Pękala *et al.*, 2003).

Based on the textures and modal composition of the less altered samples, the volcanic rocks are subdivided into the following types: 1) weakly pophyrytic, two-pyroxene lavas, including microcrystalline lavas and fine-grained lavas; and 2) plagioclase-phyric, clinopyroxene lavas.

The above petrographic subdivision correlates well with the geochemical characteristics of the volcanic rocks (Tab. 1, details in the following chapters). The petrographic and geochemical criteria combined enable the classification of even more altered samples. Consequently, a combined textural-chemical classification of the volcanic rocks is preferred in this paper (Tab. 1, column 1).

The *microcrystalline basaltic andesites* (Fig. 5A) are almost aphyric to sparsely porphyrytic (less then 5% phenocrysts up to 3 mm long). The phenocrysts are mainly represented by chlorite/smectite pseudomorphs after olivine. More rarely, plagioclase and orthopyroxene phenocrysts are observed. The microcrystalline, intersertal, often trachytic-textured groundmass consists mainly of plagioclase laths (typically < 0.2 mm long), prismatic to anhedral crystals of ortho- and clinopyroxenes, and subordinate Fe-Ti oxides and apatite. Single crystals of hornblende and biotite were observed in the groundmass of only a few samples. Anhedral alkali feldspars and quartz, and chlorites and clay minerals are found in small amounts as interstitial components, partly formed due to the replacement of volcanic glass.

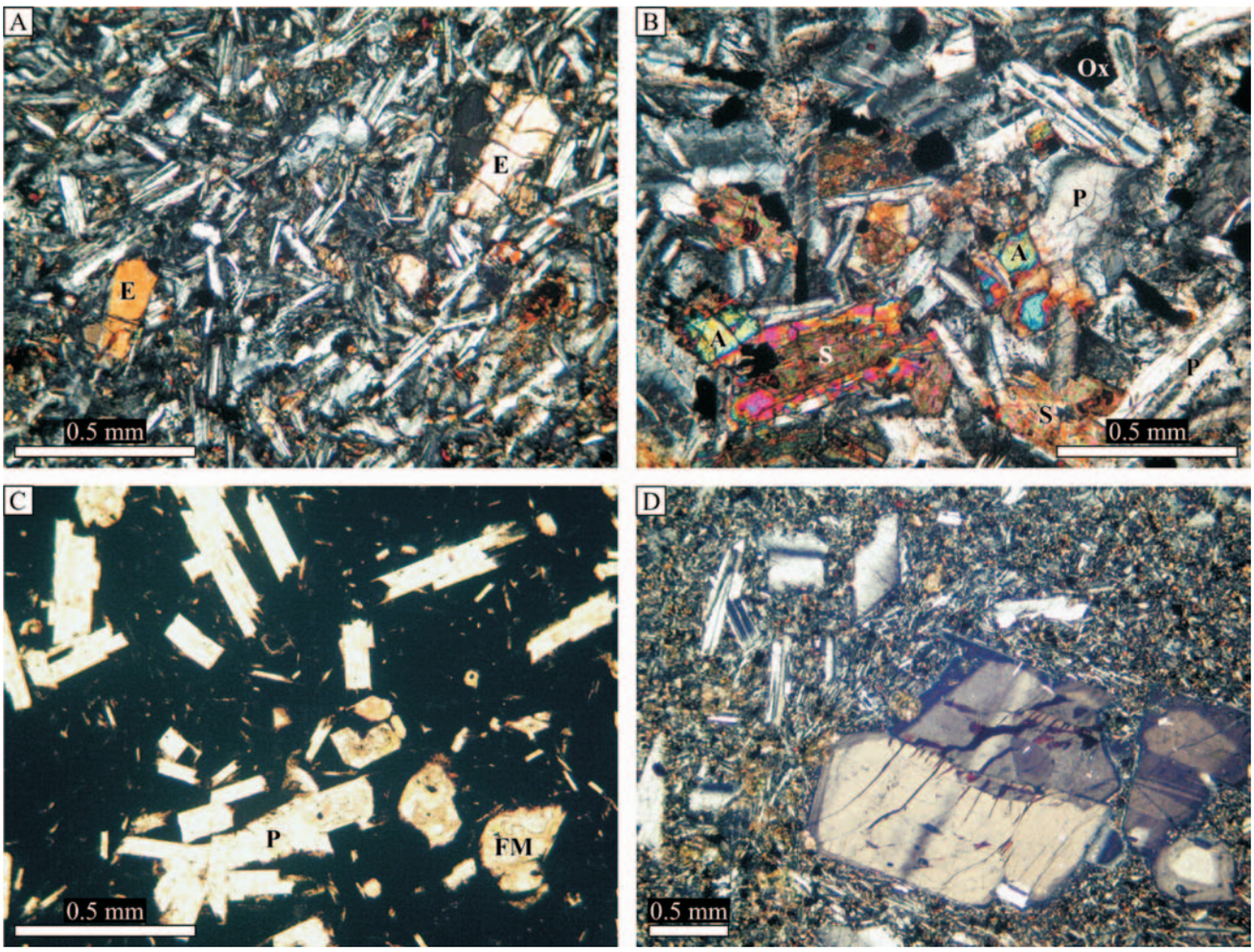

Fig. 5. Photomicrographs of the volcanic rocks. **A.** Microcrystalline basaltic andesite, crossed polars. Microphenocrysts of enstatite (E in the photo) are set in a groundmass of mainly plagioclase laths, anhedral augite and op aques. **B.** Fine-grained basaltic andesite, crossed polars. This rock is distinctly coarser-grained compared with the specimen in photo 5A and consists mainly of plagioclase (P), augite (A), Fe-Ti ox ides (Ox) and saponite (S) pseudmorphs (after orthopyroxene ?). In places (lower left) augite overgrows the saponite pseudomorphs and accicular apatite can be seen. **C.** Quench-textured basaltic andesite, plane-polarized light. This photo shows albitized plagioclase laths (P) and chlorite pseudo morphs after ferromagnesian minerals (FM) set in an opaque, hematite-stained groundmass with plagioclase microliths. Many plagioclase laths show swallow-tailed terminations (e.g. up per right). **D.** Basaltic trachyandesite, crossed polars. Zoned and twinned plagioclase phenocrysts are set in a groundmass of mainly plagioclase and clinopyroxene microliths.

The *fine-grained basaltic andesites* are characterized by a relatively coarser-grained and inequigranular texture (Fig. 5B). Plagioclase and pyroxenes are the main components, and they form prismatic to tabular crystals ca. 0.2–1.5 mm long. Orthopyroxene is rarely fresh and is typically replaced with saponite (Awdankiewicz and August, 1998). This clay mineral occurs as relatively large, well-defined mica-like plates with a perfect cleavage, greenish pleochroism and bright, second-order interference colours. In places, these pseudomorphs show overgrowths of clinopyroxene. The other components of these rocks are opaque minerals, apatite, and chlorite pseudomorphs after, most probably, olivine. The intersticies are filled with hematite-stained alkali feldspars with a felsitic to spherulitic texture. Locally, interstitial chlorites and clay minerals are also found.

Both the microcrystalline and fine-grained basaltic andesites grade into vesicular, quench-textured, originally glass-rich lavas towards the margins of the lava flows (Fig. 4C). These quenched rocks consist of phenocrysts, microphenocrysts and microliths of altered ferromagnesian minerals and plagioclase set in an almost opaque, hematite-rich matrix of altered glass. The larger plagioclase laths often show a skeletal habit or swallow-tailed terminations, and the altered glassy matrix contains numerous acicular plagioclase microliths, some of which are curved or form open, incomplete spherulites. The quenched-textured fine-grained basaltic andesites can be distinguished from the quenched-textured microcrystalline basaltic andesites by a significantly larger size of plagioclase crystals and ferromagnesian pseudomorphs in the former.

The chemical composition of the minerals in the microcrystalline and the fine-grained basaltic andesites is very similar. The plagioclase composition ranges from An68 to An45 (Fig. 6, Tab. 2). Normally zoned to almost homogeneous, as well as reversely zoned crystals were ana-

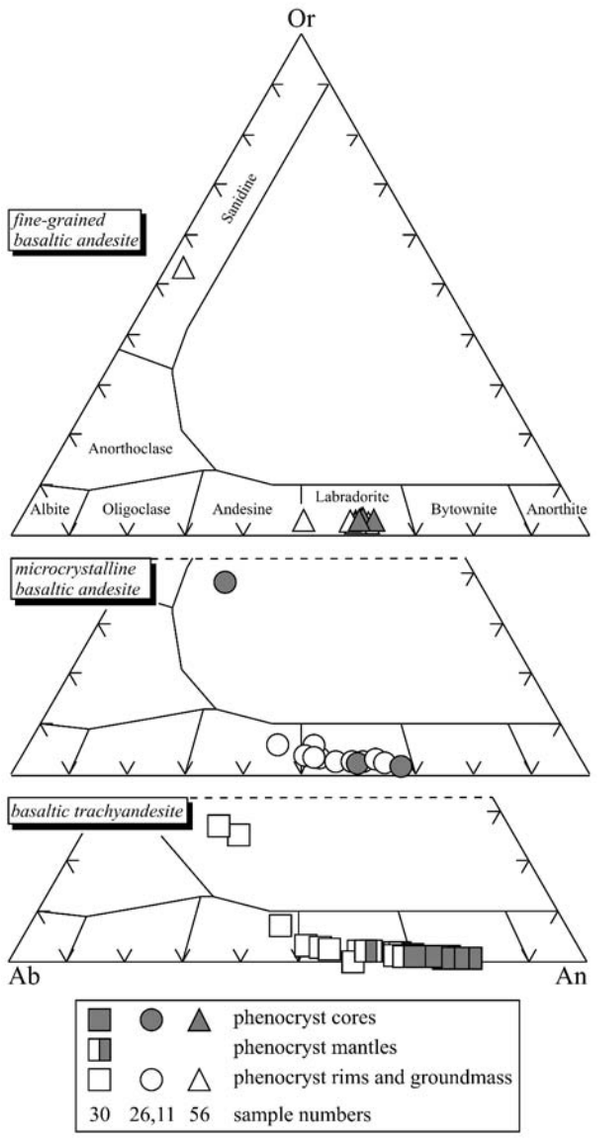

Fig. 6. The feldspar composition of the volcanic rocks on the Ab-Or-An plot (albite-orthoclase-anorthite, respectively).

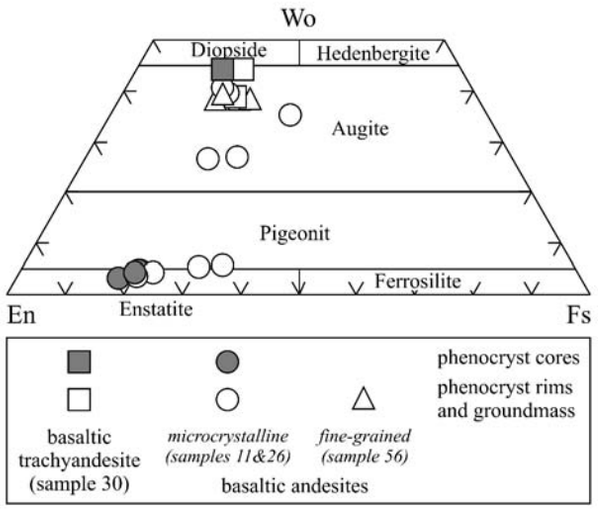

Fig. 7. The pyroxene composition of the volcanic rocks on the En-Wo-Fs plot (enstatite-wollastonite-ferrosillite, respectively).

lysed. The groundmass alkali feldspar is of a sanidine composition (Or53, Ab44, An3), and a similar ternary feldspar microphenocryst (Or38, Ab44, An 18) was analysed in one sample. The enstatite phenocrysts and groundmass crystals are Mg-rich and unzoned to normally zoned (En79-60, Fs18-34, Wo3.2-5.5), with the En-poor compositions gradational towards pigeonite (Fig. 7, Tab. 3). The groundmass clinopyroxene is represented by augite of a variable composition (En52-34, Fs17-30, Wo38-41), although the Wo-poor and Fs-rich analyses are rather rare. Fe-Ti oxides possibly comprise Ti-magnetite and ilmenite. However, no good analyses were obtained due to the degree of alteration, the small size of the crystals and the complex intergrowths with silicate minerals.

The *basaltic trachyandesites* (Fig. 5D) are characterized by porphyritic to glomeroporphyritic and seriate textures with a microcrystalline, intersertal groundmass. The phenocryst content reaches ca. 20 % (vol.) and the phenocrysts are predominantly plagioclase plates and laths up to ca. 5 mm long. Much less commonly, phenocrysts of clinopyroxene and pseudomorphs after olivine are found. The plagioclase phenocrysts typically show a normal oscillatory zoning (from An80-70 at cores down to An60-50 at rims, Fig. 6 and Tab. 2), but reverse zoning is also found (An50 at cores to An60 at rims). Rounded cores, sieve textures and small subhedral inclusions of clinopyroxene are observed in some larger plagioclase phenocrysts. The groundmass mainly consists of plagioclase laths (normally zoned, An59 to An44) with less abundant anhedral augite (Wo44-39, En41-37, Fs20-18, Fig. 7 and Tab. 3). Alkali feldspars of a ternary composition close to anorthoclase (Ab47-50, Or25-27, An23-28) are found as anhedral groundmass grains and overgrowths on plagioclase laths. Accessory minerals include small opaque crystals (probably Ti-magnetite and ilmenite; no good analyses were obtained) and apatite. Carbonates, chlorites and clay minerals, partly formed after ferromagnesian minerals and partly after interstitial glass, are found in variable amounts. Similar to the basaltic andesites, gradation into strongly altered hypocrystalline rocks is observed towards the margins of the lava flows. However, the quench textures are not well developed, and abundant plagioclase phenocrysts remain a characteristic feature of these rocks.

The described rocks are generally devoid of enclaves or xenoliths. However, strongly corroded polycrystalline quartz xenoliths (up to ca. 1 cm across) were observed in two samples of the microcrystalline basaltic andesites and in one sample of the basaltic trachyandesite.

Table 2

Representative chemical analyses of feldspars

Rock	BTa	BTa	BTa	BAm	BAm	BAm	BAm	BAm	BAm	BAf	BAf	BAf	BAf
Sample	30	30	30	26	26	11	11	11	11	56	56	56	56
Analysis	876	877	878	813	814	823	824	818	819	886	887	891	892
Mineral	Pc	Pm	Pr	Gc	Gr	Pc	Pr	MPc	MPr	MPc	MPr	MPc	MPr
oxides [%]													
SiO_2	48.47	53.73	61.79	54.76	50.61	53.32	52.96	60.00	56.21	52.19	53.57	51.95	66.91
Al_2O_3	32.14	28.88	21.88	27.48	29.14	30.57	28.67	23.30	27.83	29.14	28.45	29.00	18.00
Fe_2O_3	0.56	0.69	1.21	0.79	1.72	0.71	1.27	0.81	0.94	0.59	0.82	0.92	0.36
MnO	0.02	0.00	0.02	0.02	0.03	0.02	0.02	0.02	0.02	0.00	0.00	0.00	0.00
MgO	0.07	0.08	0.30	0.13	1.11	0.21	0.91	0.50	0.23	0.18	0.15	0.71	0.16
CaO	16.71	12.95	4.71	10.02	11.81	12.03	11.90	3.29	11.01	13.13	12.32	11.98	0.64
Na_2O	2.29	4.37	5.65	5.38	3.78	4.43	4.16	4.43	5.34	4.27	4.74	4.34	4.89
K2O	0.11	0.35	4.61	0.69	0.51	0.39	0.41	5.87	0.57	0.41	0.50	0.50	9.13
Total	100.37	101.05	100.17	99.27	98.71	101.68	100.30	98.22	102.15	99.91	100.55	99.40	100.09
cations [normalized to 8O]													
Si	2.219	2.418	2.784	2.495	2.340	2.380	2.401	2.752	2.493	2.382	2.425	2.380	3.015
Al	1.733	1.531	1.161	1.474	1.587	1.607	1.531	1.258	1.453	1.566	1.517	1.564	0.955
Fe^{3+}	0.019	0.023	0.041	0.027	0.060	0.024	0.043	0.028	0.031	0.020	0.028	0.032	0.012
Mn	0.001	0.000	0.001	0.001	0.001	0.001	0.001	0.001	0.001	0.000	0.000	0.000	0.000
Mg	0.005	0.005	0.020	0.009	0.077	0.014	0.062	0.034	0.015	0.012	0.010	0.048	0.011
Ca	0.820	0.624	0.227	0.489	0.585	0.575	0.578	0.162	0.523	0.642	0.598	0.588	0.031
Na	0.203	0.381	0.494	0.475	0.339	0.383	0.366	0.394	0.459	0.378	0.416	0.385	0.427
K	0.006	0.020	0.265	0.040	0.030	0.022	0.024	0.343	0.032	0.024	0.029	0.029	0.525
Total	5.006	5.002	4.993	5.010	5.019	5.006	5.006	4.972	5.007	5.024	5.023	5.026	4.976
X site	3.971	3.972	3.986	3.996	3.987	4.011	3.975	4.038	3.977	3.968	3.970	3.976	3.982
Z site	1.035	1.030	1.007	1.014	1.032	0.995	1.031	0.934	1.030	1.056	1.053	1.050	0.994
end members [mol%]													
Ab	19.7	37.2	50.1	47.3	35.5	39.1	37.8	43.8	45.3	36.2	39.9	38.4	43.4
An	79.7	60.9	23.0	48.7	61.3	58.7	59.7	18.0	51.6	61.5	57.3	58.7	3.2
Or	0.6	2.0	26.9	4.0	3.1	2.2	2.5	38.2	3.2	2.3	2.8	2.9	53.4

Fe_2O_3* – total iron as Fe_2O_3. Some analyses show relatively high MgO probably due to impure analysed spot. End-members (An-anorthite, Ab-albite, Or-orthoclase) calculated from cation proportions based on 8 O. Rocks: BTa – basaltic trachyandesite, BAm – microcrystalline basaltic andesite, BAf – fine-grained basaltic andesite. Minerals: P – phenocryst, MP – microphenocryst, G – groundmass, c – core, m – mantle, r – rim.

THE PETROGRAPHIC AND MINERALOGICAL CONSTRAINTS ON THE MAGMATIC PROCESSES

From the petrographic and mineralogical characteristics of the volcanic rocks given above, two main conclusions can be drawn.

1) The phenocryst assemblages of the volcanic rocks do not contain primary hydrous phases or their relics, and thus indicate a generally low water content of the magmas, consistent with the non-explosive emplacement mode of the volcanic rock, as evidenced by the geological data. The very rare hornblende and biotite is confined to the groundmass of some of the basaltic andesites and represents the products of the late stages of crystallization.

2) The major petrographic and mineralogical characteristics of the volcanic rocks, such as their phenocryst contents and assemblage, phenocryst composition and zoning pattern, and groundmass mineralogy, are very similar in the microcrystalline and fine-grained basaltic andesites, and significantly different in the basaltic trachyandesites. Consequently, it is likely that there are close genetic links between the two basaltic andesite types, and a different origin for the basaltic trachyandesites.

The differences in the mineral assemblages and mineral chemistry between the basaltic trachyandesites and the basaltic andesites possibly reflect both differences in the melt compositions and different conditions of crystallization. It is well established that the content of Ca-rich end-members in both plagioclase and clinopyroxene increases with water enrichment of the melt (Johnson *et al.*, 1994). Thus, the relatively high contents of anorthite in the plagioclase and wollastonite components in the clinopyroxene of the basaltic trachyandesites suggest that the basaltic

Table 3

Representative chemical analyses of pyroxenes

Rock	BTa	BTa	BAm	BAm	BAm	BAm	BAm	BAm	BAm	BAf	BAf
Sample	30	30	26	26	26	11	11	11	11	56	56
Analysis	898	899	832	833	834	839	840	820	841	903	904
Mineral	G	G	Pc	Pr	G	MPc	MPr	G	G	Gc	Gr
oxides [wt%]											
SiO_2	49.80	51.83	54.56	53.24	51.31	55.08	53.79	50.76	49.67	51.42	50.85
TiO_2	1.38	0.97	0.36	0.29	0.97	0.35	0.31	0.00	0.74	0.79	0.80
Al_2O_3	4.49	2.04	1.75	4.71	2.65	2.57	2.77	7.60	6.70	2.08	1.64
FeO*	10.78	11.83	12.49	11.98	9.84	12.36	13.65	9.59	14.51	10.08	12.37
MnO	0.28	0.32	0.30	0.32	0.25	0.29	0.32	0.24	0.35	0.27	0.35
MgO	12.58	14.31	26.46	25.51	14.62	27.09	24.87	12.84	15.05	15.60	14.15
CaO	20.82	18.81	2.32	2.15	19.43	2.02	2.07	16.85	12.04	18.24	18.14
Na_2O	0.40	0.46	0.11	0.17	0.34	0.18	0.23	0.98	0.32	0.74	0.86
K_2O	0.00	0.00	0.00	0.01	0.00	0.00	0.01	0.08	0.02	0.00	0.01
Total	100.53	100.57	98.35	98.38	99.41	99.94	98.02	98.94	99.40	99.22	99.17
cations [normalized to 6O]											
TSi	1.858	1.928	1.989	1.937	1.920	1.970	1.979	1.895	1.865	1.916	1.915
TAl	0.142	0.072	0.011	0.063	0.080	0.030	0.021	0.105	0.135	0.084	0.073
TFe3	0.000	0.000	0.000	0.000	0.000	0.000	0.000	0.000	0.000	0.000	0.013
T	2.000	2.000	2.000	2.000	2.000	2.000	2.000	2.000	2.000	2.000	2.001
M1Al	0.055	0.018	0.064	0.138	0.037	0.078	0.099	0.229	0.161	0.007	0.000
M1Ti	0.039	0.027	0.010	0.008	0.027	0.009	0.009	0.000	0.021	0.022	0.023
M1Fe3	0.038	0.032	0.000	0.000	0.012	0.000	0.000	0.000	0.000	0.086	0.103
M1Fe2	0.169	0.129	0.000	0.000	0.108	0.000	0.000	0.056	0.000	0.018	0.080
M1Mg	0.700	0.794	0.926	0.854	0.816	0.913	0.892	0.715	0.818	0.867	0.794
M1	1.001	1.000	1.000	1.000	1.000	1.000	1.000	1.000	1.000	1.000	1.000
M2Mg	0.000	0.000	0.512	0.529	0.000	0.532	0.472	0.000	0.025	0.000	0.000
M2Fe2	0.130	0.207	0.381	0.364	0.188	0.370	0.420	0.244	0.456	0.210	0.194
M2Mn	0.009	0.010	0.009	0.010	0.008	0.009	0.010	0.008	0.011	0.009	0.011
M2Ca	0.832	0.750	0.091	0.084	0.779	0.077	0.082	0.674	0.484	0.728	0.732
M2Na	0.029	0.033	0.008	0.012	0.025	0.012	0.016	0.071	0.023	0.053	0.063
M2K	0.000	0.000	0.000	0.000	0.000	0.000	0.000	0.004	0.001	0.000	0.000
M2	1.000	1.000	1.001	0.999	1.000	1.000	1.000	1.001	1.000	1.000	1.000
cations	4.000	4.000	4.000	4.000	4.000	4.000	4.000	3.996	3.999	4.000	4.000
end members [mol%]											
Wo	44.3	39.0	4.7	4.6	40.8	4.1	4.4	39.7	27.0	38.0	38.0
En	37.3	41.3	74.9	75.1	42.7	76.0	72.7	42.1	47.0	45.2	41.2
Fs	18.4	19.7	20.3	20.3	16.5	19.9	22.9	18.1	26.0	16.8	20.8

FeO* – total iron as FeO. End-members (Wo-wollastonite, En-enstatite, Fs-ferrosilite) calculated from cation proportions based on 6 O. Rocks: BTa – basaltic trachyandesite, BAm – microcrystalline basaltic andesite, BAf – fine-grained basaltic andesite. Minerals: P – phenocryst, MP – microphenocryst, G – groundmass, c – core, m – mantle, r – rim

trachyandesite magmas contained more water compared with the basaltic andesite magmas. Also, the more alkaline composition of the basaltic trachyandesites compared to the basaltic andesites (higher total alkalis in the former at a similar silica content) may account for the respective one-pyroxene vs. two-pyroxene mineral assemblages of these volcanic rocks. However, the occurrence of orthopyroxene phenocrysts in the basaltic andesites may also indicate their crystallization at lower pressures (= at shallower depths) compared to the basaltic trachyandesites. This is suggested by the experimental results on some compositionally similar volcanic rocks (calc-alkaline basaltic andesites and basalts) showing that low-Ca pyroxenes crystallized at low pressures only (Bakker & Eggler, 1987). In addition, the variable zoning and reaction textures in the plagioclase phenocrysts of the basaltic trachyandesites suggest some influence of disequilibrium or open-system processes, such as undercooling, degassing or magma mixing. However, the details of the physical and chemical conditions of crystallization are subject to rather speculative interpretations at present because of the post-magmatic alteration, unknown composition of the minerals such as olivine and Fe-Ti oxides, and relatively limited amount of mineralogical data obtained.

GEOCHEMISTRY

Post-magmatic alteration and element mobility

The petrographic characteristics of the Permian volcanic rocks of the North-Sudetic Basin show that a low-temperature, hydrothermal alteration strongly affected the intermediate lavas, typically resulting in the crystallization of secondary carbonates, chlorites, clay minerals and quartz. The abundance of the volatile-rich secondary minerals is well reflected in the elevated values of the loss on ignition (LOI) in the whole-rock chemical analyses of the studied rocks, and thus LOI may be used as the index of degree, and partly of the type, of alteration.

The chemical effects of alteration are illustrated in Fig. 8, where concentrations of selected elements are plotted against LOI. Samples with fresh plagioclase and pyroxene and with LOI < 2% are characterized by narrow ranges of SiO_2 and K_2O contents (52–56% and 1.5–2.5%, respectively). Altered samples in which primary igneous minerals are not present and LOI > 2% show a significantly wider scatter of SiO_2 and K_2O contents (44–62%, and 0–4.5%, respectively). The highest LOI values (up to nearly 9%) and the lowest SiO_2 contents correlate with an abundance of secondary carbonates in the studied specimens. Similarly, relatively high SiO_2 and K_2O contents at moderate LOI values are consistent with the presence of clay minerals and secondary groundmass quartz in these samples. The discussed relationships indicate that Si and K were mobile and variably enriched or depleted during the alteration processes.

TiO_2 and Cr are characterized by a different type of variation. The TiO_2 content varies from ca. 1 to 1.7%, and the same narrow range is observed in all the samples irrespective of the LOI values. The highest TiO_2 contents (ca. 1.5–1.7%) are found in the basaltic trachyandesites, both at low and high LOI values. The Cr concentrations of samples with fresh plagioclase and pyroxene and LOI < 2% vary much more widely, but this correlates well with the petrographic characteristics of the samples: the highest Cr is characteristic of the two-pyroxene lavas (with the microcrystalline lavas enriched in Cr compared with the fine-grained lavas), and the lowest Cr is found in the plagioclase-phyric lavas. The same ranges of TiO2 and Cr are seen in the altered samples with high LOI. It is concluded that the concentrations of Ti and Cr were not significantly affected by the alteration processes.

The described relationships follow the well-established general trends of mobility of major and trace elements (e.g. Winchester & Floyd, 1977). Silica, alkalis (K, Na), most other major elements (e.g. Ca, Fe, Mg), and the Large Ion Lithophile Elements (LILE: Rb, Sr, Ba) are the mobile elements, and their concentrations were variably affected during the alteration of the studied rocks of the North-Sudetic Basin. The High Field Strength Elements (HFSE: Zr, Nb, Ti, Th) and the Rare Earth Elements (REE) represent the immobile elements, and their concentrations were not significantly affected by the alteration. Cr (as well as Ni and V) are also in the category of immobile elements in the studied volcanic rocks.

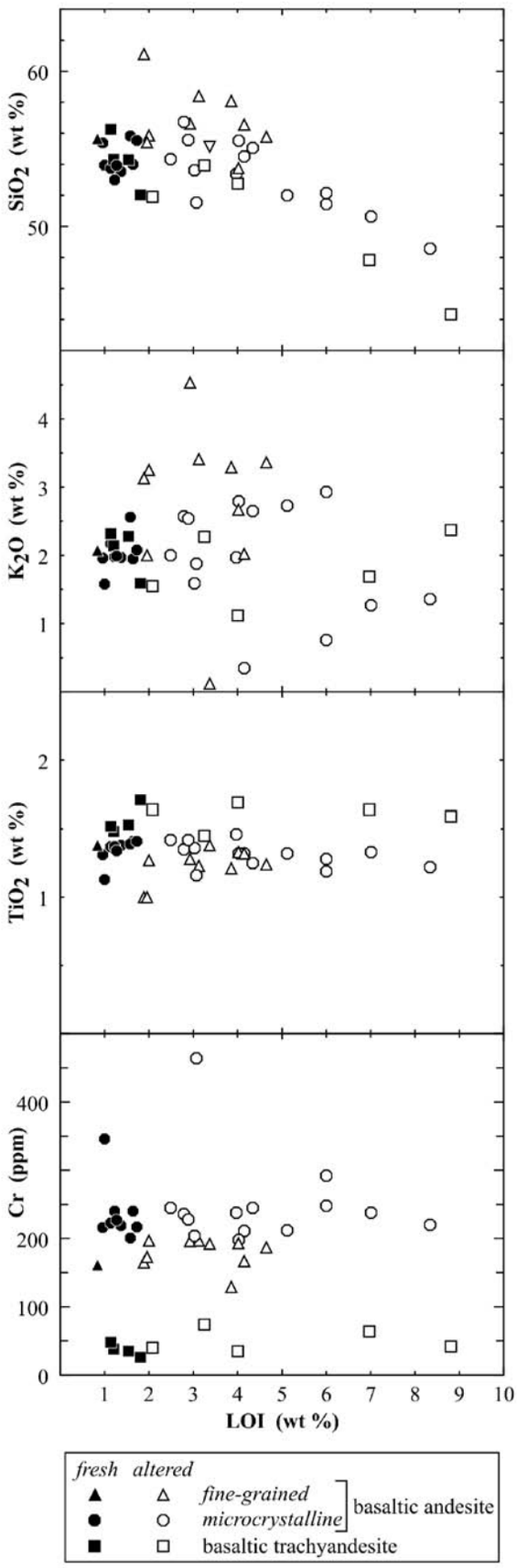

Fig. 8. The variation of selected major and trace elements in the volcanic rocks plotted against LOI (Loss On Ignition), illustrating the geochemical effects of the hydrothermal alteration. Comments in the text.

Table 4

Representative chemical analyses of the volcanic rocks

Sample	30	33	41	11	12	18	26	19	25	73
Rock	BTa	BTa	BTa	BAm	BAm	BAm	BAm	BAf	BAf	BAf
SiO_2	52.03	51.92	54.32	53.55	48.58	55.38	53.94	55.87	61.11	55.59
TiO_2	1.71	1.64	1.48	1.38	1.22	1.31	1.13	1.27	1.00	1.42
Al_2O_3	16.98	17.68	17.05	15.00	15.44	15.65	16.22	16.00	15.00	16.15
Fe_2O_3	9.84	8.07	9.48	8.96	5.82	8.63	8.21	7.54	6.53	6.83
MnO	0.19	0.18	0.08	0.12	0.19	0.13	0.25	0.15	0.09	0.06
MgO	3.54	3.01	3.64	6.05	3.57	5.91	7.43	4.83	2.23	4.27
CaO	8.52	10.12	6.92	7.01	12.78	7.13	7.94	2.59	3.45	6.58
Na_2O	3.28	3.36	3.63	2.94	2.75	2.83	2.43	5.08	4.00	3.03
K_2O	1.59	1.55	2.14	1.97	1.36	1.96	1.58	3.25	3.13	2.54
P_2O_5	0.62	0.56	0.53	0.56	0.00	0.00	0.36	0.47	0.45	0.00
LOI	1.81	2.08	1.21	1.37	8.34	0.96	1.00	2.00	1.89	2.89
total	100.11	100.17	100.48	98.91	100.05	99.89	100.49	99.05	98.88	99.36
Mg#	41.60	42.48	43.42	57.21	54.85	57.56	64.19	55.92	40.35	55.32
Cr	26	40	38	219	220	216	346	197	165	228
Ni	37	46	24	155	127	112	172	125	88	152
Co	48	67	48	48	45	51	58	45	45	47
Sc	20	21	21	19	22	21	23	17	17	20
V	150	170	135	127	155	135	155	123	104	123
Cu	40	24	19	18	49	30	91	10	19	14
Pb	15	20	30	20	24	22	19	49	54	30
Zn	94	105	200	89	163	87	74	295	41	234
W	101	220	128	82	111	125	141	130	208	106
Rb	40	39	62	57	36	57	30	87	130	76
Ba	717	575	506	538	276	504	430	612	616	493
Sr	333	345	311	294	243	280	249	202	291	291
Cs	0.5	0.8	1.1	0.7	1.4	1.1	0.5	0.9	4.9	1.3
Zr	328	302	315	370	265	329	247	390	381	402
Hf	6.5	6.2	5.9	4.5	5.4	5.9	5.3	7.1	7.2	4.7
Y	42	40	41	45	34	41	33	46	41	46
Nb	28	27	27	30	22	27	22	29	27	32
Ta	2.0	2.0	1.5	1.6	1.3	1.9	1.3	1.9	1.6	1.7
Th	5.1	5.0	6.5	7.7	6.6	7.3	6.5	10.7	11.1	8.2
U	1.0	1.2	1.2	1.5	1.3	1.3	1.0	1.9	1.5	1.2
La	45.2	43.8	47.5	55.1	46.6	50.5	39.1	61.1	60.6	65.0
Ce	96	92	100	117	94	108	85	127	122	129
Nd	46	44	43	55	41	49	38	60	55	60
Sm	8.24	8.04	8.25	9.38	7.44	8.73	6.74	9.88	9.40	10.50
Eu	2.27	2.12	2.03	2.36	1.86	2.10	1.60	2.05	1.98	2.55
Tb	1.20	1.20	1.10	1.30	1.00	1.20	1.00	1.40	1.30	1.50
Yb	3.55	3.54	3.41	3.74	3.04	3.71	3.00	3.86	3.21	4.13
Lu	0.55	0.53	0.48	0.55	0.49	0.54	0.42	0.57	0.44	0.60

BTa – basaltic trachyandesite, BAm – microcrystalline basaltic andesite, BAf – fine-grained basaltic andesite. A general sample location is shown in Fig. 2. The list below gives detailed locations in the form: [sample number; locality; topographic coordinates]; the coordinates are after the Państwowy Układ Współrzędnych 1965. Samples: [11; Sędziszowa; 645.85, 556.09], [12; Lubiechowa; 644.68, 552.53], [18; Bucze Małe; 644.30, 554.48], [19; Sokołowiec; 643.88, 556.74], [25; Stefanów; 640.95, 556.89], [26; Stefanów; 640.48, 556.13], [30; Sołtysia Czuba; 638.21, 557.05], [33; Góra Folwarczna; 633.59, 557.63], [41; Górczyca; 632.15, 559.66], [73; Mogiła; 624.04, 562.05].

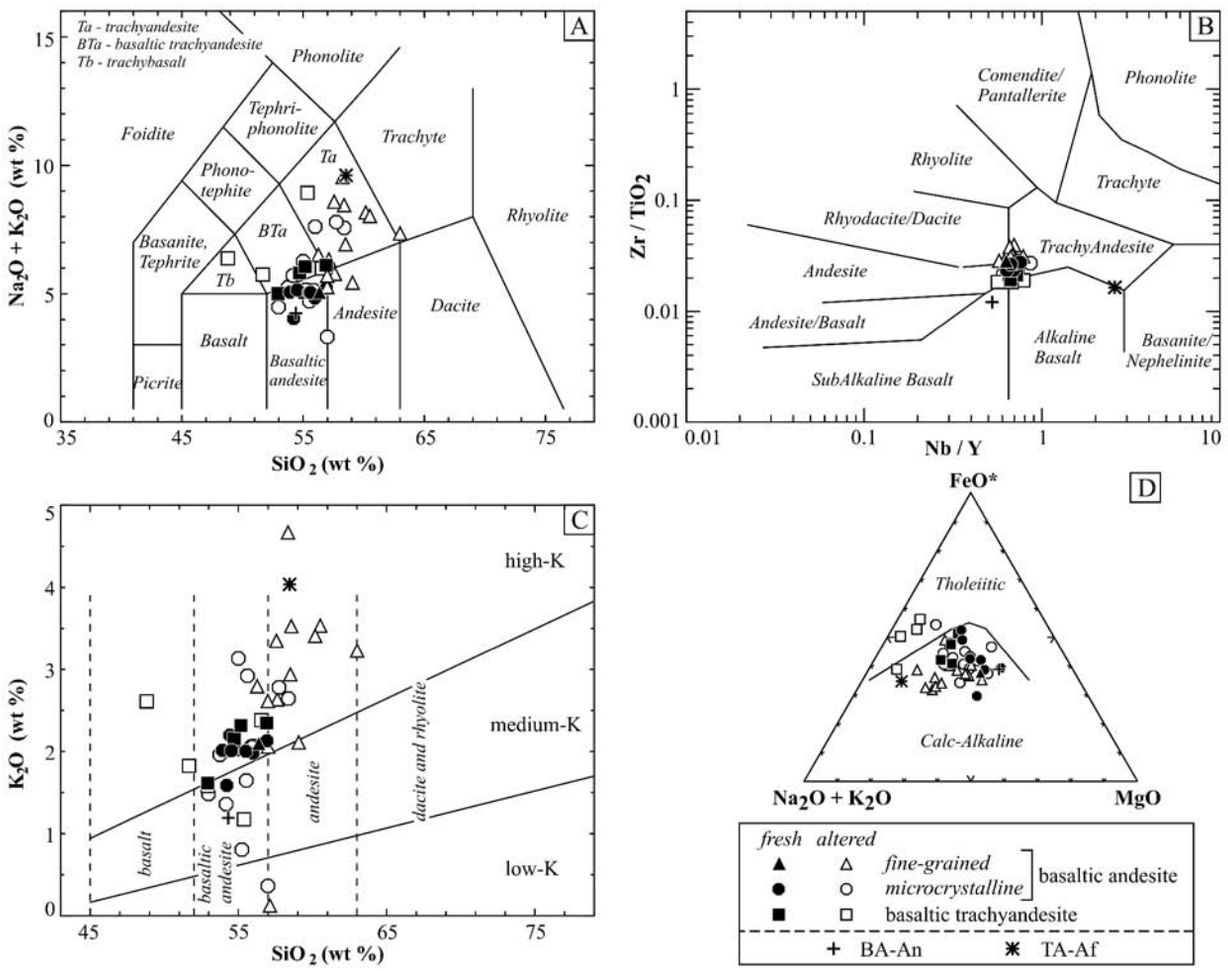

Fig. 9. The chemical classification of the volcanic rocks. **A.** The total alkali-silica diagram (TAS) after Le Maitre (Ed.) (2002). **B.** The Zr/TiO2-Nb/Y plot after Winchester & Floyd (1977). **C.** The K2O-SiO2 plot after Le Maitre (Ed.) (2002). **D.** The AFM plot after Irvine & Baragar (1971). In all the diagrams, two samples of recent volcanic rocks are plotted for comparison: BA-An – basaltic andesite, Central Volcanic zone, Andes; and TA-Af – trachyandesite, the East African Rift System (details in the text).

Consequently, the geochemical characterization and genetic interpretation of the volcanic rocks in the following chapters, as well as the numerical modelling of the chemical evolution of the magmas, are essentially based on the immobile elements. When the mobile elements are used (e.g. for the chemical classification of volcanic rocks) only the fresh samples are considered significant. The fresh samples, as used hereafter in this paper, are those which show both petrographic and geochemical evidence of freshness: 1) a lack of significant alteration in the pyroxenes and plagioclase, and 2) LOI < 2%. 14 samples of the 43 analysed for geochemistry were thus classified as fresh. The discussed geochemical data (Fig. 8) and the other diagrams further on in this paper show that the 14 fresh samples are representative of the whole sample set (cover the compositional spectrum of the whole set).

The geochemical characteristics of the volcanic rocks

Chemical analyses of representative samples of the volcanic rocks are shown in Table 4. Fig. 9. shows the chemical classification diagrams of the volcanic rocks. In the Zr/TiO_2-Nb/Y diagram of Winchester and Floyd (1977), used for the classification of altered and metamorphosed volcanic rocks, the Permian lavas of the North-Sudetic Basin form an aligned, tight cluster that straddles the boundary of several classification fields. Because of relatively small variation in the Zr, Ti, Nb and Y ratios, and their specific values, this diagram was not very helpful in the classification of the studied rocks. However, this plot indicated the intermediate composition (basaltic to andesitic) and the transitional, subalkaline/alkaline affinity of this suite (the Nb/Y ratio of 0.67 is suggested as the boundary value between the subalkaline and alkaline basalts by Winchester and Floyd, 1977). In the TAS and K_2O-SiO_2 diagrams, the data plotted with a wider distribution. However, this scatter was probably due to the mobility of the silica and alkalis on alteration, as the fresh samples showed a much more restricted compositional range. The enrichment in silica and alkalis typical of the altered samples is probably due to the crystallization of secondary quartz, albite and clay minerals replacing plagioclase and volcanic glass, the main primary components of these rocks (see the previous chapters).

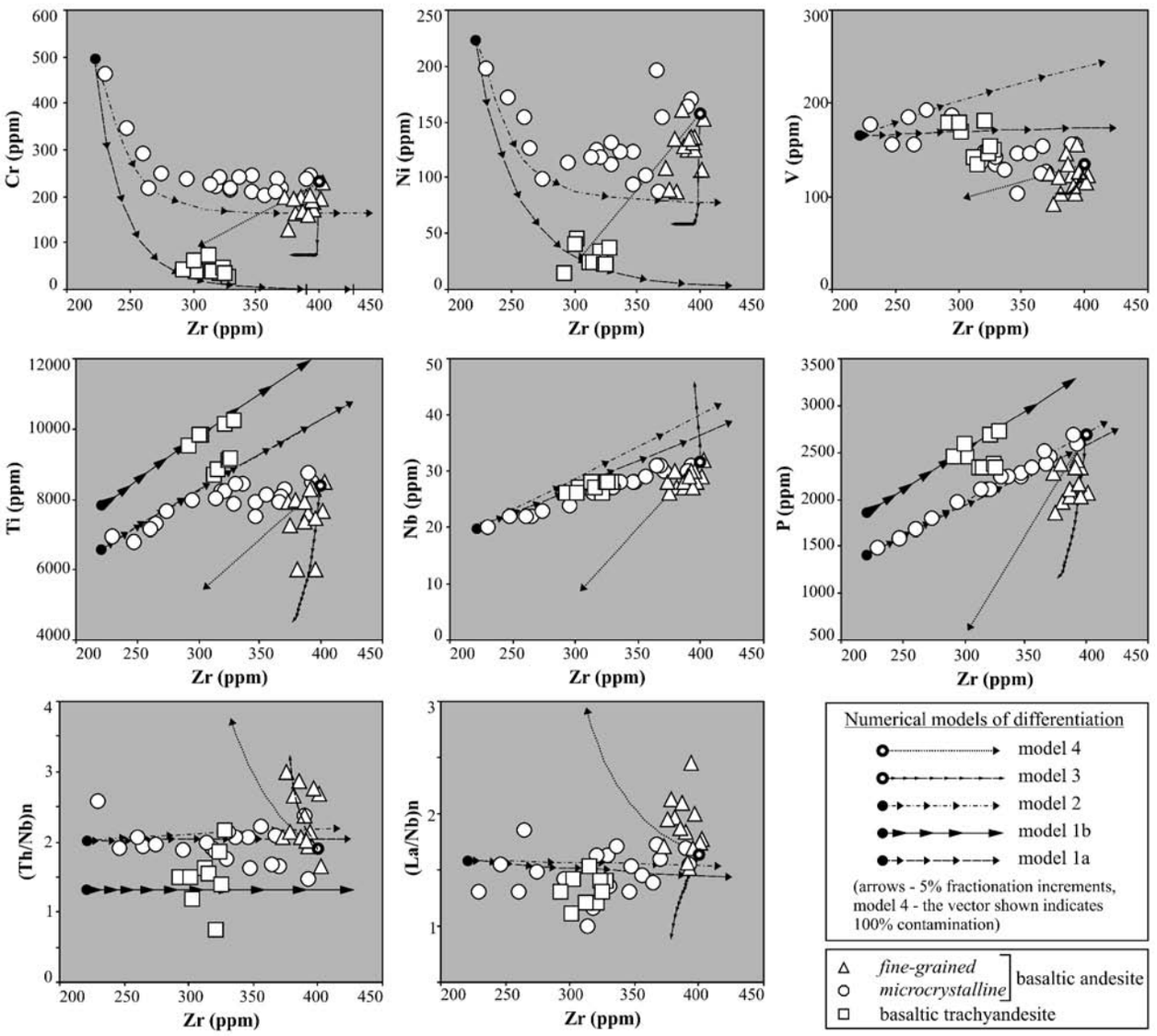

Fig. 10. The variation in selected trace element contents and ratios of the volcanic rocks plotted against the Zr content. (Th/Nb)n and (La/Nb)n are primitive mantle-normalized ratios (Wood et al., 1979). Also plotted are numerical models of differentiation, see the text and Appendix 1.

Consistently with the moderate Nb/Y ratios, the fresh samples also plot along the boundary of the subalkaline and alkaline suites in the TAS diagram (Fig. 9). The AFM and K_2O-SiO_2 diagrams show the calc-alkaline and high-K affinity of this suite, respectively. From the TAS plot, the two-pyroxene lavas are classified as basaltic andesites, and further subdivided into main series basaltic andesites (the microcrystalline lavas) and evolved basaltic andesites (the fine-grained lavas, Tab. 1). There is a gradation between the two types of basaltic andesites in terms of their major element compositions. The plagioclase-phyric lavas are enriched in alkalis at a silica level similar to the basaltic andesites, and are classified as basaltic trachyandesites.

In terms of their silica contents (52–57%), Mg# ratios (< 0.7), and Ni and Cr contents (< 200 ppm and < 470 ppm, respectively), the volcanic rocks represent moderately evolved magma compositions (Tab. 4). The geochemical variation is further illustrated in Fig. 10. The Zr content is plotted at the horizontal axis as the differentiation index. The Cr-Zr plot enables a clear distinction to be made between the basaltic trachyandesites characterized by the lowest Cr contents, and the basaltic andesites characterized by higher Cr contents and a well-defined inflected Cr-Zr trend. The microcrystalline basaltic andesites plot along the low-Zr and the main part of that trend, while the fine-grained basaltic andesites plot at the Zr-rich end, usually showing some depletion in Cr. Similar relationships are found between Ni and Zr, although there is a greater scatter, possibly due to a variable Ni enrichment of the samples containing olivine phenocrysts. In addition, a systematic up-sequence increase in Zr and Cr contents is observed in the Pławna2, Wleń and Lubiechowa sections (Fig. 3B). This variation, together with the field and petrographic data (see previous chapters) points to systematic changes in the lava compositions during the eruptive episodes.

The basaltic andesites are characterized by positive, linear correlations between Zr and several other incompatible trace elements. The Zr-P and Zr-Nb trends for the micro-crystalline basaltic andesites are almost perfectly linear (Fig. 10, correlation coefficients R2 = 0.9842 and 0.9559, respectively), and less distinctive, inflected or more scattered for other element pairs (e.g. Zr-Ti). Compared to the microcrystalline basaltic andesites with a similar Zr content, the fine grained basaltic andesites show distinctive depletion in P, Nb and Ti (Fig. 10), and enrichment in Th and LREE over Nb (higher Th/Nb and La/Nb ratios, Fig. 10). By contrast, the basaltic trachyandesites show enrichment in Ti, P (and much less clear in Nb), and depletion in Th (relatively low Th/Nb ratio, Fig. 10).

Normalized REE patterns of representative samples are shown in Fig. 11. The patterns are subparallel and show negative slopes, relatively steep La-Sm segments, and flatter Tb-Lu segments. These features indicate a distinctive LREE enrichment relative to the MREE and HREE, and a less pronounced MREE enrichment over the HREE. In the microcrystalline basaltic andesites, with increasing Zr contents, the REE contents systematically increase (Fig. 11A) at almost constant normalized Ce/Yb ratios of ca. 7.7 (Fig. 11B). The fine-grained basaltic andesites show the strongest LREE enrichment (chondrite-normalized Ce/Yb up to ca. 10), while the basaltic trachyandesites are less enriched (chondrite-normalized Ce/Yb down to ca. 6.5). All these rocks are also characterized by a small negative Eu anomaly which is rather indistinct in the basaltic trachyandesites (highest Eu/Eu* up to 0.94), clearer in the microcrystalline basaltic andesites (mean Eu/Eu* = 0.89), and most pronounced in the fine-grained basaltic andesites (lowest Eu/Eu* down to 0.72).

Primitive mantle-normalized trace element patterns of the volcanic rocks are shown in Fig. 12A. The patterns of all the rock types distinguished are very similar, sub-parallel, with generally negative slopes and several negative anomalies. These patterns indicate relative enrichment in LILE and LREE over HFSE and selective depletion in such elements as Sr, Ti, Nb, Ta, P, Hf, Cs and U. The patterns shown include the potentially mobile LIL elements, but the samples are fresh (low LOI, unaltered plagioclase and pyroxenes) except for sample 19. However, even this altered sample shows the LILE pattern very similar to the other, fresh rocks (e.g. the Th-U-K-Ta segment) and documents the highest LILE content in the fine-grained basaltic andesites.

Two samples of recent intermediate-composition volcanic rocks are plotted in Fig. 12A for comparison. Sample BA-An is a calc-alkaline basaltic andesite representative of the Central Volcanic Zone of the Andes, and sample TA-Af is an alkaline trachyandesite representative of the East African Rift system (from Wilson, 1989, tables 7.3 and 11.3). These two samples were selected for comparison because: 1) they broadly bracket the compositional range of the studied Permian suite in terms of major element composition (Fig. 9); and 2) they may be considered representative of intermediate lavas of active continental margins (sample BA) and intra-continental extensional settings (sample TA). The studied Permian rocks show normalized

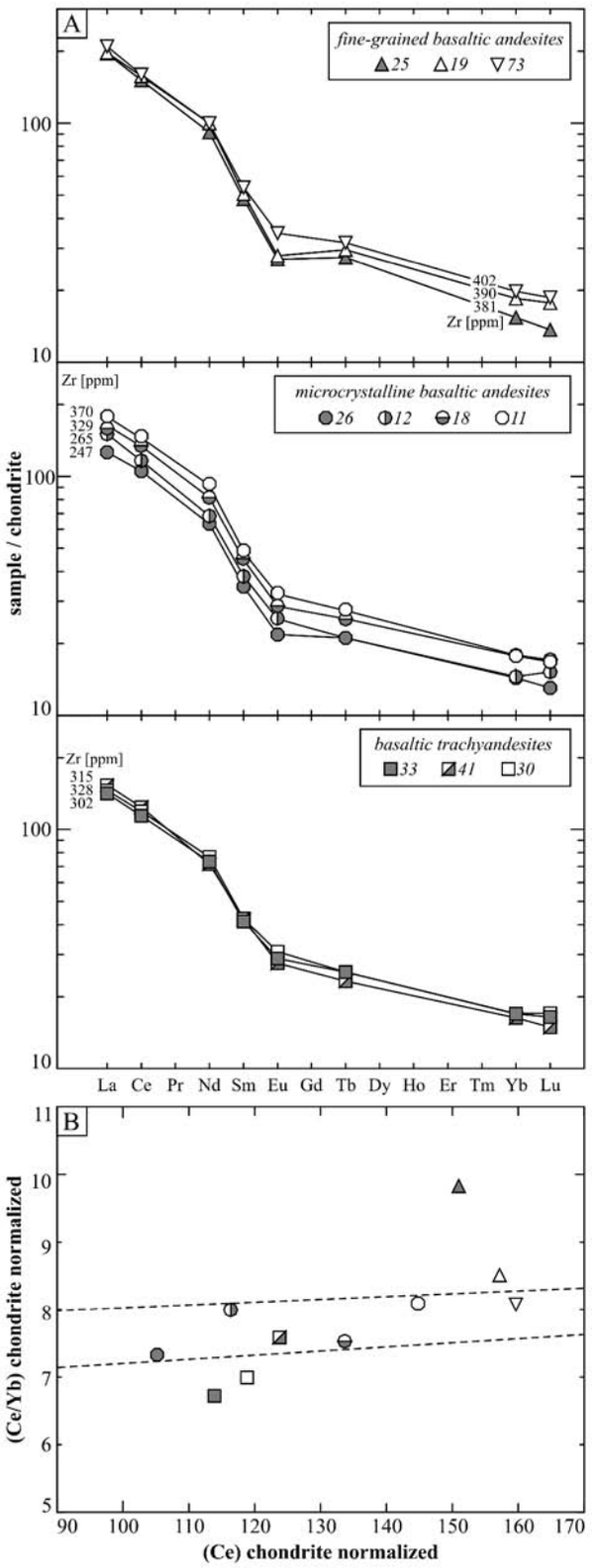

Fig. 11. The rare-earth element (REE) geochemistry of the volcanic rocks. A. Chondrite-normalized REE patterns. B. (Ce/Yb) normalized ratio plotted against normalized (Ce). The broken lines delineate the range of (Ce/Yb) ratios in the microcrystalline basaltic andesites. Normalization after Boynton (1984).

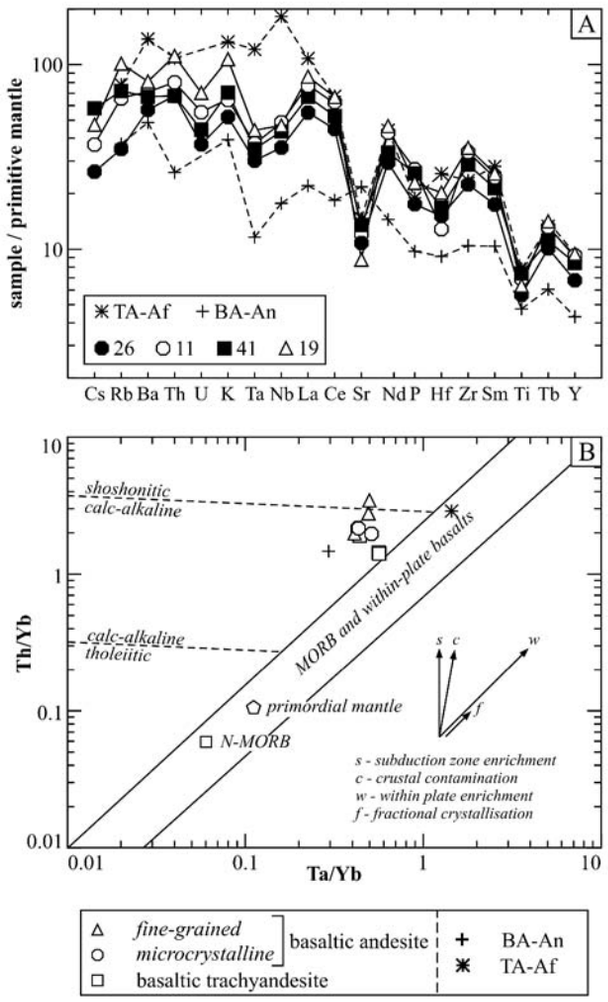

Fig. 12. A. Primitive mantle-normalized (after Wood et al., 1979) trace element patterns of the volcanic rocks. **B.** The Th/Yb-Ta/Yb diagram of Perace (1983). In both diagrams, two samples of recent volcanic rocks are plotted for comparison: BA-An – basaltic andesite, Central Volcanic zone, Andes; and TA-Af – trachyandesite, the East African Rift System (details in the text).

patterns from La to Y generally similar to sample TA in terms of both their trace element ratios and contents. However, sample TA shows a strong enrichment in Nb and Ta, while the Permian rocks show depletion in these elements relative to K and La, similarly as in sample BA. The LIL element contents and ratios of the Permian samples are gradational between samples BA and TA. This comparison shows that the Permian lavas of the North-Sudetic Basin show trace element characteristics transitional between extension-related within-plate lavas, and active continental margin lavas. These transitional characteristics are also seen in the Th/Yb-Ta/Yb plot (Fig. 12B) where the studied rocks show high Ta/Yb ratios typical of within-plate lavas, but also elevated Th/Yb ratios characteristic of destructive plate margin lavas.

MAGMA DIFFERENTIATION PROCESSES

Qualitative interpretation

Overall, the volcanic rocks show very uniform geochemical characteristics and relatively narrow ranges of variation of several major and trace elements, as evidenced, for example, by the tight clustering of points in the TAS (the fresh samples) and Zr/TiO_2-Nb/Y classification diagrams, and also by the subparallel spider diagrams. These characteristics indicate that the discussed rocks represent a suite of genetically related magmas, derived from very similar parental melts and, ultimately, similar mantle sources. The relatively high silica and low magnesium contents suggest that even the more primitive of the analysed compositions may not represent primary, unmodified mantle magmas but rather variably evolved melts. However, the samples with the lowest Zr, and highest Mg-, Cr- and Ni contents may approximate the parental magma composition of this suite. The major differentiation process involved in the evolution of this suite must have been fractional crystallization, as indicated by the progressive enrichment in incompatible trace elements such as Zr, Nb, P, REE, at constant ratios of these elements, correlated with the relative depletion in compatible elements as such Cr, Ni, V and Eu (Figures 10, 11, 12). These depletions further indicate the fractional crystallization of olivine, pyroxenes, Fe-Ti oxides and plagioclase. However, for several elements in Fig. 10, the variation diagrams reveal complex trends, suggesting that other processes apart from fractional crystallization were also influential during the magmatic evolution of this suite.

In particular, the inflections in the Cr-Zr, Ni-Zr and Ti-Zr trends for the basaltic andesites at ca. 270–300 ppm of Zr may reflect some changes in the fractionating mineral assemblages, e.g. from Cr-spinel-bearing assemblages in the less evolved (Zr-poor) magmas into Ti-spinel- or ilmenite-bearing assemblages in the more evolved (Zr-enriched) magmas, fractionating Cr and Ti, respectively. However, another possible explanation is a continuous replenishment of the magma chamber where the fractional crystallization processes took place with a primitive, Cr- and Ni-rich magma, buffering the compatible element contents at a high level. Another characteristic feature is the depletion in Ti, Nb and P, and enrichment in Th and La relative to Nb in the basaltic andesites with the highest Zr contents. These trends can be linked with fractional crystallization of some accessory minerals from the more evolved melts (e.g. apatite and zircon, incorporating P and Zr, respectively), and/or contamination of the fractionating magmas with some crustal material (Nb-poor and Th and LREE-rich). In addition, the basaltic trachyandesites represent a distinctive group in many of the variation diagrams shown (Fig. 10). Their strong depletion in Cr and Ni reflects advanced fractional crystallization of ferromagnesian minerals and/or Fe-Ti oxides (and no influence of mafic replenishment). The sub-trends (parallel to the main, basaltic andesite trend) observed in the Ti-Zr and P-Zr diagrams

also suggest that the basaltic trachyandesites were derived from parental magmas of slightly different composition compared to the parental magmas of the basaltic andesites.

Numerical modelling

The possible effects of the various differentiation processes discussed above were tested quantitatively using simple numerical models. Several models were calculated based on the observed rock compositions and their mineral assemblages, and those which best fit the observed trends are shown in Fig. 10. The equations applied and the data used in the modelling, including melt compositions, fractionating mineral assemblages and mineral-melt partition coefficients, are given in Appendix 1. Importantly, the models are considered only a rough approximation of the natural differentiation processes, as many complexities cannot be incorporated into the simple equations used (e.g. gradual changes in fractionating mineral assemblages), and some of the partition coefficients used (e.g. for apatite and zircon in basic/intermediate melts) are not constrained well.

Model 1a represents the fractional crystallization of plagioclase, olivine, clinopyroxene and minor spinel from a parental magma with a composition close to the Zr-poorest and Cr-richest sample of the data set (Cc(1a) in App. 1C). Models with orthopyroxene in the fractionating mineral assemblage (not shown) give similar results. Model 1b (calculated for selected elements only) illustrates the fractional crystallization of the same mineral assemblage but from a slightly different parental melt (Cc(1b) in App. 1C).

Models 1a and 1b show that fractional crystallization of a mineral assemblage equivalent to the phenocryst assemblage observed in the basaltic trachyandesites explains well the formation of basaltic trachyandesite magmas from more primitive melts ranging in composition from the least evolved basaltic andesites to (hypothectical) slightly more alkaline, Ti- and P-enriched, magmas. A range of parental magma compositions involved explains best the distinctive basaltic trachyandesite sub-trends in the Ti-Zr and P-Zr plots, and also the variation in the Th/Nb and La/Nb ratios measured in these rocks. However, some of these parental magmas were not erupted and/or not sampled, and their real composition remains poorly constrained. Although the calculated models give similar results if either clinopyroxene or orthopyroxene are involved, the petrographic evidence argues for the crystallization of clinopyroxene and not orthopyroxene.

Model 2 represents fractional crystallization coupled with the replenishment of the magma chamber with a primitive melt. This process was modelled using the assimilation-fractional crystallization (AFC) equation, with the initial melt composition representing the magma contained in the chamber (Cc(1a), the same parental melt as used in model 1a) and the assimilant being the primitive magma that replenished the chamber (Cp, App. 1C). The composition of the latter, hypothetical magma was calculated by extrapolating from the basaltic andesite trends to lower Zr contents assuming Cr = 1000 ppm in the primary, mantle-derived magma (after Wilson, 1989). The fractionating mineral assemblage consisted of plagioclase, orthopyroxene, olivine and minor spinel. It is found that such models require a very high Cr content in the replenishing magma batches (partly depending on the partition coefficients applied, but not much less than 1000 ppm) and high ratios of mass assimilated to mass fractionated: ca. 0.8, i.e. voluminous replenishment with the primitive melt. Models with clinopyroxene in the fractionating mineral assemblage (not shown) fail to reproduce the observed trends because clinopyroxenes fractionate Cr which leads Cr-depleted melts, despite the mafic replenishment. Another set of models tested assumed a two-step fractional crystallization, with or without the mafic replenishment, with a change of mineral assemblages at ca. 300 ppm of Zr. These models (not shown) also failed to reproduce the high Cr and Ni of the evolved basaltic andesites, unless the fractionated assemblages in step 2 (Zr > 300 ppm) consisted almost exclusively (> 90%) of plagioclase, which is unrealistic for the magma compositions involved.

It is thus considered that model 2 confirms that the geochemical variation of most trace elements in the basaltic andesites can be explained by fractional crystallization of plagioclase, olivine and orthopyroxene, with minor spinel (which compares well with the phenocryst assemblage and modal composition of the basaltic andesites), coupled with massive replenishment of the magma chamber with a very primitive melt. However, the variation of Ti, V and partly Nb probably requires the onset of crystallization of a Ti-V-Nb-bearing phase, likely ilmenite, at a fractionation degree corresponding to ca. 300 ppm of Zr. This relatively complex case (fractional crystallization + replenishment + variation of mineral assemblages) cannot be easily modelled because the equation used is valid for a constant value of the bulk partition coefficient, which effectively means that no changes in the fractionating mineral assemblage are allowed.

Model 3 represents fractional crystallization of an evolved basaltic andesite magma (Cc3, App. 1C) coupled with the replenishment of the magma chamber with the primitive melt. Similarly to model 2, the AFC equation was used. The fractionating mineral assemblage was also similar to that in model 2 (Pl, Opx, Ol, Sp), but included very small fractions of ilmenite, apatite and zircon. Due to the poorly constrained partition coefficients for the latter two minerals in the basic/intermediate melts (App. 1E) model 3 provides only a very general guide to possible fractionation paths.

It is found that relatively small changes in the mineral proportions, partition coefficients and assimilation/fractionation ratio strongly influence the resulting chemical trends. The model presented semi-quantitavely demonstrates that the co-variation of several trace elements (e.g. Zr, Ti, V, P) in the most evolved basaltic andesites can be explained by fractional crystallization of the accessory minerals. However, the P depletion in that model requires apatite crystallization, which also leads to LREE depletion due to the high partition coefficients of the LREE such as La in apatite. Consequently, the model predicts that the La/Nb ratio of the most evolved melts should decrease,

but the opposite effect is observed in the studied suite. Thus, it seems likely that the fractional crystallization of accessory minerals, if it occurred, was not the only process involved at that stage of differentiation.

The last model, 4, illustrates the effects of crustal contamination and represents a linear two-end-member mixing between the evolved basaltic andesite magma and a mean greywacke composition (compositions Cc3 and Ca, respectively, App. 1C). Other contaminants tested included the average lower crust, the average upper crust and the NASC (North American Shale Composite). None of these compositions provide a perfect fit to the observed trends. However, contamination of the evolved basaltic andesite magma with a relatively mafic, immature sedimentary component (= greywacke) or a partial melt of such a source, explains relatively well the variation in Zr, Nb, P, Cr and the increase in the Th/Nb and La/Nb ratios of the most evolved basaltic andesites. In conclusion, it is suggested that the most evolved magmas of the suite were affected by both fractional crystallization of accessory minerals and also by crustal assimilation.

The evolution of the magmatic systems

The field relationships and the petrographic and geochemical variation in the volcanic rocks discussed in this paper can be integrated into a model that shows how the magmatic systems of the Permian volcanoes of the North-Sudetic Basin worked and evolved with time. The main processes involved are schematically illustrated in Fig. 13. The parental magmas of the suite differentiated in crustal chambers and erupted effusively in several episodes separated by repose periods. The parental magma compositions and, more significantly, magma chamber processes changed with time during the eruptive episodes, and successive lavas showed a systematic up-sequence geochemical and petrographic variation. The lavas that erupted early (stage I in Fig. 13) were of relatively low volume and of basaltic trachyandesite composition. At that stage, the magmas evolved primarily by the fractional crystallization of plagioclase, clinopyroxene and olivine from the primitive melts, leading to the Cr-poor compositions. In the following, main eruptive stage (II), the volumetrically dominant microcrystalline basaltic andesite lavas were emplaced. The parental magma composition shifted to slightly less alkaline. The magma chambers possibly attained a larger size due to a more continuous and more voluminous supply, and might have been located at shallower crustal levels. The melts evolved by fractional crystallization of plagioclase, orthopyroxene and olivine (with minor Fe-Ti oxides: Cr-spinel first, titanomagnetite or ilmenite later), coupled with mixing of evolved and primitive replenishing melts, leading to the Cr-rich compositions. The assimilation of crustal materials did not occur during stages I and II, and constant ratios of incompatible trace elements (e.g. Zr/P, Zr/Nb, Th/Nb) of the melts were maintained. Progressive differentiation resulted in still more evolved melts, and the most evolved, fine-grained basaltic andesite lavas were produced and emplaced during the final stage, III. As in the previous stage, the main differentiation processes remained fractional crystallization and mafic replenishment, but the trace element characteristics of the magmas were affected by the fractional crystallization of accessory minerals (e.g. zircon and apatite) and also by contamination with upper crustal components that were similar in composition to greywackes. These processes resulted in the depletion of Zr, Cr, Nb and P, and enrichment in Th and La.

Similar eruptive episodes consisting of stages I-II-III, or some of the stages only, were repeated several times as volcanism resumed after repose periods. Several magma chambers evolving in a similar way must have been successively created underneath the volcanic centres. The most complete spectrum of erupted lava compositions was characteristic of the volcanoes in the central part of the North-Sudetic Basin. By contrast, further east, where the intermediate lavas are associated with rhyolites, the basaltic trachyandesite lavas did not erupt, and so the evolved basaltic andesites are relatively more common. The rhyolites possibly reflect a more extensive crustal melting beneath volcanoes in the east, which both prevented the rise of initial, low-volume basaltic trachyandesite magmas to the surface, and also favoured a more advanced differentiation in the magma chambers, leading to the more common emplacement of the evolved basaltic andesite lavas.

Some aspects of the proposed model remain less clear. For instance, the lavas of stage I (basaltic trachyandesites) bear stronger petrographic evidence of disequilibrium crystallization (plagioclase zonation), suggestive of open system processes, compared to lavas of stage II (basaltic andesites). However, a larger magma chamber, a longer residence time for the magmas, and a resulting more thorough homogenization of the stage II melts could account for these characteristics. Another problem is why crustal assimilation occurred at the very late stage of differentiation only. It can be speculated that both magma chamber processes (e.g. a decrease in the magma supply and/or the formation of a thick cumulate pile, disabling effective replenishment) and wall rock processes (e.g. melting of the country rocks only after enough heat was supplied from the cooling magma chamber) contributed to this situation.

THE MANTLE SOURCES, CRUSTAL COMPONENTS AND PARENTAL MAGMAS OF THE SUITE

Although the volcanic rocks of the North-Sudetic Basin represent rather evolved melts, some basic characteristics of their mantle sources and other components involved in their petrogenesis can be discussed. The enrichment in the more incompatible elements of the HFS group, documented by the relatively high Nb/Y, Nb/Zr and Ta/Yb ratios, indicates derivation of the melts from moderately enriched mantle sources. The REE patterns, in particular the lack of HREE depletion (high chondrite-normalized Yb concentrations of ca. 16) further suggest

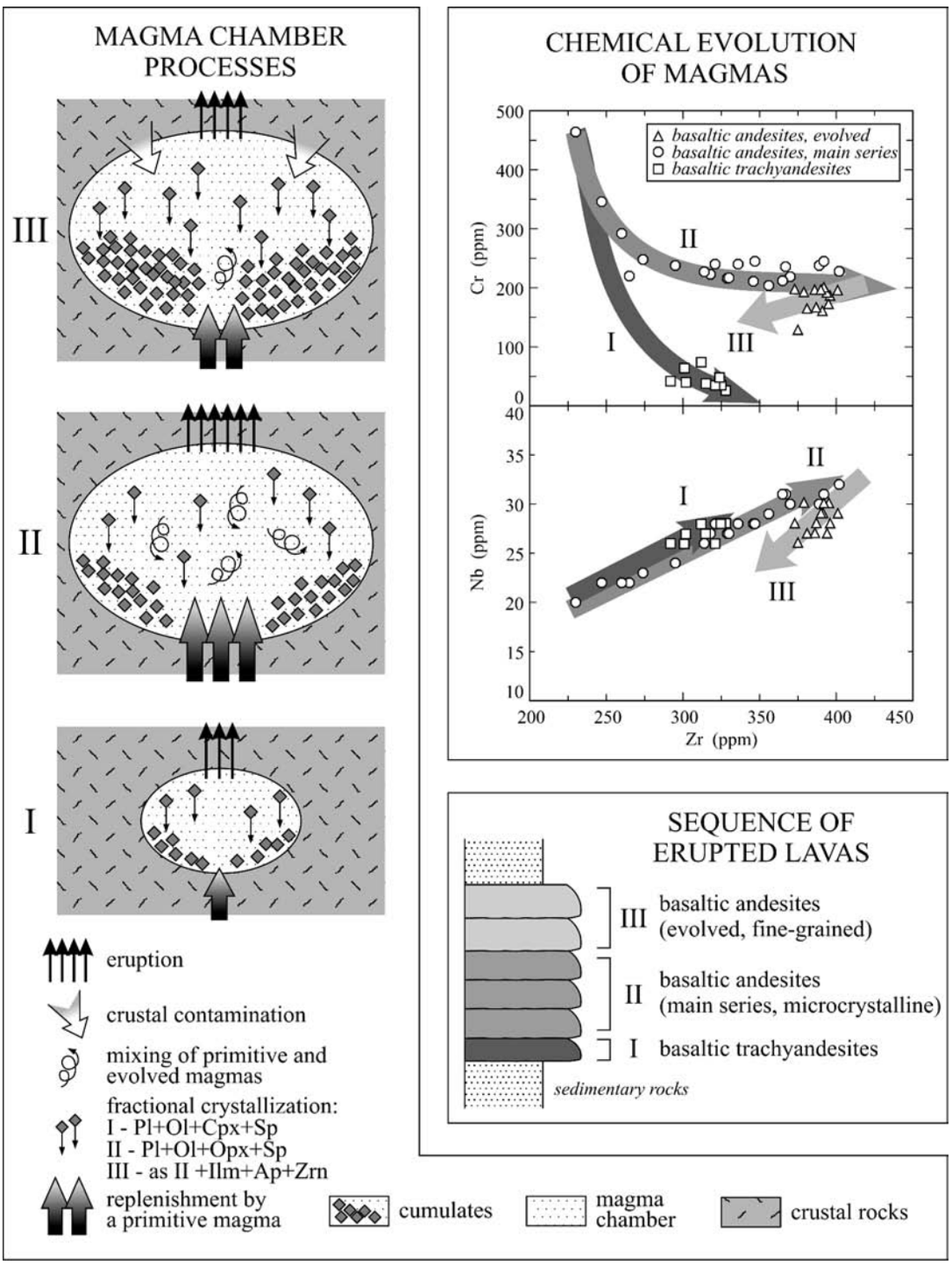

Fig. 13. An illustration of the magmatic evolution of the Permian volcanic rocks of the North-Sudetic Basin, including magma chamber processes, the chemical evolution of magmas and the emplacement sequence of the lavas.

that garnet was absent from the mantle sources of the magmas, likely due to the rather shallow origin of the melts (at pressures lower than those required for the stability of garnet-peridotite assemblages) and/or relatively high degrees of partial melting. Altogether, it may be argued that the magmas were derived from trace element-enriched, spinel-peridotite sources located in the subcontinental lithospheric mantle. In addition, the geochemical differences between the basaltic andesites and the basaltic trachyandesites suggest also some heterogeneity of the mantle source and/or variation in the degrees of partial melting for the various parental magmas.

However, unlike typical continental intra-plate lavas (e.g. sample TA-Af, Fig. 12) showing low La/Nb and Th/Nb ratios, the discussed Permian rocks are characterized by distinctive enrichement in Th, LILE and La over

Nb, similar to active continental margin lavas (e.g. sample BA-An in Fig. 12). These enrichments indicate that some components rich in Th, LILE and LREE, most probably crustal rocks and/or fluids derived from such rocks, participated in the origin of the magmas. The possible mechanism involved could have been:

1) contamination of the magmas during their differentiation within the crust, or

2) contamination of the mantle source of the magmas by subduction-related fluids or deeply subducted crustal rocks.

A strong contamination of the Permian "andesites" of the North-Sudetic Basin with lower crustal rocks as the result of assimilation-fractionation processes was suggested by Dziedzic (1998). However, these suggestions were based on a very limited set of 5 samples, and the geochemical and petrographic variation of the "andesites" was not recognized; thus, the model presented by Dziedzic (1998) must be treated with caution. By contrast, the data discussed in this paper and the results of numerical modelling of trace element variation show that:

1) crustal contamination was not involved until the most advanced stages of differentiation, and

2) the magma chambers were replenished with very primitive (= undifferentiated) magmas, which could hardly have suffered any earlier fractionation or contamination.

These arguments suggest that the trace element signatures of the discussed suite were largely inherited from the mantle sources. Considering the post-collisional setting, it is possible that the mantle sources were contaminated during the earlier stages of the Variscan orogeny either due to subduction-related metasomatism or due to a deep subduction of crustal rocks, as also suggested for other similar, post-colllisinal rock series (e.g. Cabanis *et al.*, 1990; Benek *et al.*, 1996; Aldanmaz *et al.*, 2000; Coulon *et al.*, 2002).

CONCLUSIONS

1. The Permian intermediate-composition volcanic rocks of the North-Sudetic Basin represent a high-K calc-alkaline suite that erupted in an extensional, intracontinental, post-collisional setting in the eastern part of the Variscan belt of Europe.

2. The volcanic rocks, with a total volume exceeding a hundred cubic km, are mostly thick pahoe-hoe lava flows and minor subvolcanic intrusions that were emplaced from fissure vents and/or small shield-type volcanoes. Locally, the lavas interacted with wet sediments producing peperites and pillow-like structures. An idealized, single eruptive episode comprised initial emplacement of basaltic trachyandesite lavas, followed by main series basaltic andesites (the most voluminous and widespread), and finally, evolved basaltic andesites. Several eruptive episodes separated by repose and sedimentation periods can be recognized.

3. The geochemical, petrographic and mineralogical data indicates that the suite represents co-magmatic, variably evolved melts, coming from magmatic systems in which the differentiation processes changed with time from: (I) fractional crystallization leading to the basaltic trachyandesite compositions, through (II) fractional crystallization coupled with mafic replenishment, leading to the Cr- and Ni-rich main-series basaltic andesites, to (III) fractional crystallization, mafic replenishment and crustal assimilation producing P-, Ti- and Nb-depleted, but Th- and La-enriched evolved basaltic andesites. Importantly, the fractionating mineral assemblages changed from (I) plagioclase, olivine and clinopyroxene with minor spinel, to (II) plagioclase, olivine and orthopyroxene with minor spinel and later ilmenite, and (III) as in the previous stage, but with apatite and zircon. The most evolved basaltic andesites underwent some contamination with crustal components with greywacke-like chemical affinities. Some variation in the parental magma compositions of successive magmatic products may reflect source heterogeneity and/or variable melting conditions.

4. The general trace element characteristics of the volcanic rocks (enrichment in Th, LILE, Nb and Zr, but with high Th/Nb and La/Nb ratios) are transitional between those of extension-related within-plate lavas and active continental margin lavas. These characteristics reflect the enriched lithospheric mantle sources of the magmas, carrying a crustal signature possibly related to subduction processes (mantle metasomatism or deep subduction of crustal rocks) during the earlier stages of the Variscan orogeny.

Acknowledgements

I wish to thank Prof. J. Winchester and Prof. P. Floyd for their help with the XRF analyses at Keele University. I am grateful to Prof. R. Kryza and Mr. H. Siagło, MSc., for their assistance with the microprobe analyses at the University of Wrocław. The microprobe was donated by the Free University of Amsterdam. Prof. R. Kryza, Prof. M. Roden and Prof. A. Muszyński are gratefully acknowledged for their helpful comments to this paper. I wish also to thank Prof. C. Breitkreuz and Prof. A. Muszyński for valuable discussions during our field trips to the North-Sudetic Basin. The study was supported by the Institute of Geological Sciences, University of Wrocław (grant 1017/S/ING).

Appendix 1. Numerical modeling – methods and data

A. Equations used (based on Wilson, 1989 and Ragland, 1989 and references therein)

fractional crystallization

$C = Cc * F(D-1)$

assimilation-fractional crystallization (AFC)

$C = Cc * [f' + r/(r-1+D) * Cp(1-f')/Cc]$

and

bulk mixing

$C = (1-x)Cc + xCa$

where:

C – the calculated concentration of a given trace element in the fractionated melt

Cc – the initial concentration of that trace element in the magma in the chamber

Cp – the concentration of that trace element in the primitive magma replenishing the chamber

Ca – the concentration of that trace element in the assimilated crustal material

D – the bulk partition coefficient for the fractionating mineral assemblage

F – the fraction of the melt remaining

$f' = F-(r-1+D)/(r-1)$

r – the ratio of the assimilation rate to fractionation rate

x – the weight fraction of the assimilated material

B. Models applied

Models 1a and 1b – fractional crystallization, with Cc(1a) and Cc(1b) as the initial melt compositions, respectively

Model 2 – assimilation/fractional crystallization (AFC) with Cc(2) as the initial melt composition and Cp as the "assimilant" (replenishing primitive magma)

Model 3 – assimilation/fractional crystallization (AFC) with Cc(3) as the initial melt composition and Cp as the "assimilant" (replenishing primitive magma)

Model 4 – bulk mixing between Cc(3) and Ca

C. Melt compositions

[ppm]	Cp	Cc(1a, 2)	Cc(1b)	Cc(3)	Ca(4)
Zr	128	221	221	400	302
Ti	2792	6598	7800	8380	5400
Nb	14.3	19.8	19.8	32	8.4
Th	4.7	6.2	4	9.3	9
La	27	36	36	60	34
Ni	428	225	225	158	24
V	143	165	165	135	98
Cr	1000	500	500	229	88
P	770	1416	1850	2684	572

Cp – primitive magma replenishing the chamber

The Zr content of this magma (= 128 ppm) was calculated from the extrapolation of the linear regression of Cr against Zr for Cr = 1000. The other element contents were extrapolated from their linear regressions vs Zr for Zr = 128 ppm. The regression equations were based on 5 basaltic andesite samples with the lowest Zr contents (< 250 ppm) for most elements except Ti, Th and La, for which 4 samples were used (because of anomalous Ti, Th and La contents in the sample with lowest Zr content, see Fig. 10).

Cc(1a, 1b, 2) – the initial magma composition in the chamber in models 1a, 1b and 2, respectively. The composition calculated as for Cp assuming Cr = 500 ppm, which gives Zr = 221 ppm in the chamber magma. In Cc(1b), the Ti, P and Th contents are set arbitrarily to illustrate the possible range of magma chamber compositions.

Cc(3) – initial magma composition in the chamber in model 3

This composition was extrapolated from linear regressions of the modeled elements against Zr for basaltic andesites with Zr > 250 ppm assuming Zr = 400 ppm in the chamber magma.

Ca(4) – assimilated crustal material in model 4

The composition of a mean greywacke after Wedepohl (1995) was used.

D. Fractionating mineral assemblages and assimilation/fractionation ratios (weight fractions)

model	Ol	Opx	Cpx	Pl	Mag	Ilm	Ap	Zrn	r
1a & 1b	0.30	-	0.19	0.485	0.025	-	-	-	0
2	0.15	0.35	-	0.490	0.010	-	-	-	0.8
3	0.15	0.34	-	0.466	0.040	0.002	0.0015	0.00015	0.7

Ol – olivine, Opx – or thopyroxene, Cpx – clinopyroxene, Pl – plagioclase, Mag – magnetite, Ilm – ilmenite, Ap – apatite, Zrn – zircon

E. Mineral/melt partition coefficients

	Ol	Opx	Cpx	Pl	Mag	Ilm	Ap	Zrn
Ti	0.02	0.1	0.4	0.04	7.5	192	0.1	-
Zr	0.012	0.18	0.1	0.048	0.1	0.29	0.1	3000*
Nb	0.01	0.15	0.005	0.01	0.4	2.3	0.1	50*
Th	-	-	0.03	0.01	-	0.00055		76.8
La	0.07	0.01	0.1	0.14	2.2	0.098	14.5	16.9
Ni	17	5	8	-	29	3.8	-	-
V	0.06	0.6	1.35	-	26	12	-	-
Cr	0.7	10	34	-	153	6	-	189.5
P	0.055	0.0115	0.069	0.019	-	0.05	500*	-

Ol, Opx, Cpx, Pl, Mag, the elements Ti to Cr: partition coefficients in basaltic and basaltic andesite melts, values from the compilation of Rollinson (1993). Values for P from Baker and Wyllie (1992, for Cpx) and from Anderson and Greenland (1965, for Ol, Opx, Pl. Mag).

Ilm – values from the compilation of R. Nielsen (http://earthref.org/): Ti – Stimac and Hickmott (1994); Zr, Th – Zack and Brumm (1998); Nb – Green and Pearson (1987); La – Paster *et al*., 1974; Ni – Ewart and Griffin (1994); Cr, V – Ringwood, 1970; P – Anderson and Greenland (1965).

Ap, Zrn: partition coefficients in rhyolitic melts from the compilation of Rollinson (1993). * – P in Ap, and Zr and Nb in Zrn – arbitrary values.

REFERENCES

ALDANMAZ, E., PEARCE, J. A. , THIRLWALL, M. F. & MITCHELL, J. G., 2000. Petrogenetic evolution of late Cenozoic, post-collision volcanism in western Anatolia, Turkey. *Journal of Volcanology and Geothermal Research*, 102: 67–95.

ALEKSANDROWKI, P., KRYZA, R., MAZUR, S., PIN C. & ZALASIEWICZ, J. A., 2000. The Polish Sudetes: Caledonian or Variscan ? *Transactions of the Royal Society of Edinburgh*, 90: 127–146.

ANDERSON, A. T. & GREENLAND, L. P., 1969. Phosphorous fractionation diagrams as a quantitative indicator of crystallization differentiation of basaltic liquids. *Geochimica et Cosmochimica Acta*, 33: 493–505.

AWDANKIEWICZ, M. & AUGUST, C., 1998. Pomagmowe krzemiany warstwowe w bazaltowych andezytach i trachyandezytach czerwonego spągowca niecki północnosudeckiej. [in Polish only]. *Polish Mineralogical Society, Special Papers*, 10: 54–56.

AWDANKIEWICZ, M., 1999a. Volcanism in a late Variscan intramontane trough: Carboniferous and Permian volcanic centres of the Intra-Sudetic Basin, SW Poland. *Geologia Sudetica*, 32: 13–47.

AWDANKIEWICZ, M., 1999b. Volcanism in a late Variscan intramontane trough: the petrology and geochemistry of the Carboniferous and Permian volcanic rocks of the Intra-Sudetic Basin, SW Poland. *Geologia Sudetica*, 32: 83–111.

BAKER, M. B. & WYLLIE, P. J., 1992. High-pressure apatite solubility in carbonate-rich liquids – implications for mantle metasomatism. Geochimica et Cosmochimica Acta, 56(9): 3409–3422.

BAKKER, D. R. & EGGLER, D. H., 1987. Compositions of anhydrous and hydrous melts coexisting with plagioclase, augite and olivine or low-Ca pyroxene from 1 atm to 8 kbar: Application to the Aleutian volcanic centre of Atka. *American Mineralogist*, 72: 12–28.

BARANOWSKI, Z., HAYDUKIEIWCZ, A., KRYZA, R., LORENC, S., MUSZYŃSKI, A., SOLECKI, A. & URBANEK, Z., 1990. Outline of the geology of the Góry Kaczawskie (Sudetes, Poland). *Neues Jahrbuch für Geologie und Paläontologie Monatshefte*, 179: 223–257.

BENEK, R., KRAMER, W., MCCANN, T., SCHECK, M., NEGENDANK, F. J. W., KORICH, D., HUEBSHER, H-D. & BAYER, U., 1996. Permo-Carboniferous magmatism of the Northeast German Basin. *Tectonophysics*, 266: 379–404.

BOYNTON, W. R. 1984. Geochemistry of the rare earth elements: meteorite studies. In: Henderson P., (ed.). *Rare Earth Element Geochemistry.* Elsevier, Amsterdan, 63–114.

CABANIS, B., COCHEMÉ, J. J., VELLUTINI, P. J., JORON, J. L. & TREUIL, M., 1999. Post-collisional Permian volcanism in northwestern Corsica: an assessment based on mineralogy and trace element geochemistry. *Journal of Volcanology and Geothermal Research*, 44: 51–67.

COLLINS, A. S., KRYZA, R. & ZALASIEWICZ, J., 2000. Macrofabric fingerprints of Late Devonian – Early Carboniferous subduction in the Polish Variscides, the Kaczawa complex, Sudetes. *Journal of the Geological Society, London*, 157: 283–288.

COULON, C., MEGARTSI, M., FOURCADE, S., MAURY, R. C., BELLON, H., LOUNI-HACINI, A., COTTEN, J., COUTELLE, A. & HERMITTE, D., 2002. Post-collisional transition from calc-alkaline to alkaline volcanism during the Neogene in Oranie (Algeria): magmatic expression of a slab breakoff. *Lithos*, 62: 87–110.

DZIEDZIC, K., 1998. Genesis and evolution of Sudetic late Hercynian volcanic rocks inferred from trace element modelling. Geologia Sudetica, 31: 79–91.

EWART, A. & GRIFFIN, W. L., 1994. Application of proton-microprobe data to trace-element partitioning in volcanic-rocks. *Chemical Geology*, 117(1-4): 251–284.

FLOYD, P. A. & CASTILLO, P. R., 1992. Geochemistry and petrogenesis of Jurassic ocean crust basalts, ODP Leg 129, site 801. In: Larson R, Launcelot Y *et al.* (eds). *Proceedings of Ocean Drilling Program, Scientific Results, 129, College Station TX*: 361–388.

FRANKE, W. & ŻELAŹNIEWICZ, A., 2000. The eastern termination of the Variscides: terrane correlation and kinematic evolution. In: Franke W, Haak V, Oncken O, Tanner D (eds). Orogenic Processes: Quantification and modelling in the Variscan Belt. *Geological Society, London, Special Publications*, 179: 63–86.

GREEN, T. H. & PEARSON, N. J., 1987. An experimental study of Nb and Ta partitioning between Ti-rich minerals and silicate liquids at high pressure and temperature. *Geochimica et Cosmochimica Acta*, 51: 55–62.

IRVINE, T. N. & BARAGAR, W. R. A., 1971. A guide to the chemical classification of the common volcanic rocks. *Canadian Journal of Earth Sciences*, 8: 523–548.

JOHNSON, M. C., ANDERSON, A. T. & RUTHERFORD, M. J., 1994. Pre-eruptive volatile contents of magmas. In: Caroll MR, Holloway JR (eds). Volatiles in magmas. *Reviews in Mineralogy*, 30: 281–330.

KOWALSKA, S. & MICHALIK, M., 1996. Produkty krystalizacji pomagmowej w wulkanitach permskich z Dolnego Śląska. [in Polish only]. *Polish Mineralogical Society, Special Papers*, 8: 59–61.

KOZŁOWSKI, S. & PARACHONIAK, W., 1967. Wulkanizm permski w depresji północnosudeckiej. [in Polish, English summary]. *Prace Muzeum Ziemi, Prace Petrograficzne i Geologiczne*, 11: 191–221.

LE MAITRE, R. W., BATEMAN, P., DUDEK, A., KELLER, J., LAMEYRE, J., LE BAS, M. J., SABINE, P. A., SCHMID, R., SORENSEN, H., STREICKEISEN, A., WOOLEY, A. R. & ZANETTIN, B., 2002. *A classification of volcanic rocks and glossary of terms. Recommendations of the International Union of Geological Sciences Subcomission on the Systematics of Igneous Rocks.* Blackwell, Oxford, pp. 1–236.

LORENZ, V. & NICHOLLS, I. A., 1984. Plate and intraplate processes of Hercynian Europe during the Late Palaeozoic. *Tectonophysics*, 107: 25–56.

LORENZ, V. & NICHOLLS, I. A., 1976. The Permo-Carboniferous basin and range province of Europe. An application of plate tectonics. In: Falke H (ed). *The continental Permian in central, West and South Europe.* Dordrecht, pp. 313–342.

MAZUR, S., ALEKSANDROWSKI, P., KRYZA, R. & OBERC-DZIEDZIC, T., 2006. The Variscan Orogen in Poland. *Geological Quarterly*, 50, 89–118.

MENARD, G. & MOLANR, P., 1988. Collapse of Hercynian Tibetan Plateau into a late Palaeozoic European Basin and Range Province. *Nature*, 334: 235–237.

MILEWICZ, J., 1965. Czerwony spągowiec okolicy Lwówka Śląskiego. [in Polish, English summary]. *Biuletyn IG 185 (Z badań geologicznych na Dolnym Śląsku, t. XI)*: 195–228.

PASTER, T. P., SCHAUWECKER, D. S. & HASKIN, L. A., 1974. The behavior of some trace elements during solidification of the Skaergaard layered series. *Geochimica et Cosmo-*

chimica Acta, 38(10): 1549–1577.

PEARCE, J. A., 1983. Role of the subcontinental lithosphere in magma genesis at active continental margins. In: Hawkesworth CJ, Norry JM (eds). *Continental basalts and mantle xenoliths. Shiva, Nantwich*, pp. 230–249.

PĘKALA, M., WÓJTOWICZ, A. & MICHALIK, M., 2003. Post-eruptive history of Lower Permian volcanic rock (trachybasalt from Lubiechowa; the North-Sudetic Basin). *Polish Mineralogical Society, Special Papers*, 23: 145–147.

RAGLAND, P. C., 1989. *Basic Analytical Petrology.* Oxford University Press, pp. 369.

RINGWOOD, A. E., 1970. Petrogenesis of Apollo 11 basalts and implications for lunar origin. *Journal of Geophysical Research*, 75(32): 6,453–6,479.

ROLLINSON, H. R., 1993. *Using Geochemical Data: Evaluation, Presentation, Interpretation.* Longman Scientific & Technical, pp. 1–352.

ROMER, R., FÖRSTER, H-J. & BREITKREUZ, C., 2001. Intracontinental extensional magmatism with a subduction fingerprint: the late Carboniferous Halle Volcanic Complex (Germany). *Contributions to Mineralogy and Petrology*, 141: 201–221.

SEGHEDI, I., DOWNES, H., PÉCSKAY, Z., THIRLWALL, M. F., SZUKÁCS, A., PRYCHODKO, M. & MATTEY, D., 2001. Magmagenesis in a subduction-related post-collisional volcanic arc segment: the Ukrainian Carpathians. *Lithos*, 57: 237–262.

STIMAC, J. & HICKMOTT, D., 1994. Trace-element partition-coefficients for ilmenite, ortho-pyroxene and pyrrhotite in rhyolite determined by micro-pixe analysis. *Chemical Geology*, 117(1-4): 313–330.

ULRYCH, J., PESEK, J., STEPANKOVA-SVOBODOVA, J., BOSAK, P., LLOYD, F. E., VON SECKENDORFF, V., LANG, M. & NOVAK, J. K., 2006. Permo-Carboniferous volcanism in late Variscan continental basins of the Bohemian Massif (Czech Republic) geochemical characteristics. *Chemie der Erde, Geochemistry*, 66: 37–56.

WEDEPOHL, K. H., 1995. The composition of the continental crust. *Geochimica et Cosmochimica Acta*, 59: 1217–1239.

WILSON, M., 1989. *Igneous Petrogenesis.* Chapman & Hall, London, Glasgow, Hew York, Tokyo, Melbourne, Madras, pp. 1–465.

WILSON, M., NEUMANN, E. -R., DAVIES, G. R., TIMMERMANN, M. J., HEERMANS, M. & LARSEN, B. T., 2004. Permo-Carboniferous Magmatism and Rifting in Europe. *Geological Society Special Publication*, 223, pp. 498.

WINCHESTER, J. A. & FLOYD, P. A., 1977. Geochemical discrimination of different magma series and their differentiation products using immobile elements. *Chemical Geology*, 20: 325–343.

WOJEWODA, J. & MASTALERZ, K., 1989. Ewolucja klimatu oraz autocykliczność i allocykliczność sedymentacji na przykładzie osadów kontynentalnych górnego karbonu i permu w Sudetach. [in Polish, English abstract]. *Przegląd Geologiczny*, 4: 173–180.

WOOD, D. A., JORON, J. L., TREUIL, M., NORRY, M. & TARNEY, J., 1979. Elemental and Sr isotope variations in basic lavas from Island and the surrounding ocean floor. *Contributions to Mineralogy and Petrology*, 70: 319–339.

ZACK, T. & BRUMM, R., 1998. Ilmenite/liquid partition coefficients of 26 trace elements determined through ilmenite/clinopyroxene partitioning in garnet pyroxene. In: Gurney J. J., Gurney J. L., Pascoe M. D. & Richardson S. H. (Editors): *7th International Kimberlite Conference.* Red Roof Design, Cape Town. 986–988.